

Determinants of *de novo* B cell responses to drifted epitopes in post-vaccination SARS-CoV-2 infections

Grace E. Quirk^{1,*}, Marta V. Schoenle^{2,*^}, Kameron L. Peyton², Jennifer L. Uhrlaub²,
Branden Lau³, Jefferey L. Burgess⁴, Katherine Ellingson⁵, Shawn Beitel⁴, James
Romine⁴, Karen Lutrick⁶, Ashley Fowlkes⁷, Amadea Britton⁷, Harmony L. Tyner⁸, Alberto
J. Caban-Martinez⁹, Allison Naleway¹⁰, Manjusha Gaglani¹¹, Sarang Yoon¹², Laura
Edwards¹³, Lauren Olsho¹³, Michael Dake¹⁴, Bonnie J. LaFleur¹⁵, Janko Ž. Nikolich^{15,16},
Ryan Sprissler³, Michael Worobey^{1,15,#}, and Deepta Bhattacharya^{2,15,17,#}

¹ Department of Ecology and Evolutionary Biology, University of Arizona, Tucson, AZ,
USA

²Department of Immunobiology, University of Arizona College of Medicine, Tucson, AZ,
USA

³ University of Arizona Genomics Core and the Arizona Research Labs, University of
Arizona Genetics Core, University of Arizona, Tucson, AZ, USA

⁴ Mel and Enid Zuckerman College of Public Health, University of Arizona, Tucson,
Arizona, USA

⁵ Department of Epidemiology and Biostatistics, Zuckerman College of Public Health,
University of Arizona, Tucson

⁶ College of Medicine-Tucson, University of Arizona, Tucson, Arizona, USA

20 ⁷ National Center for Immunization and Respiratory Diseases, Centers for Disease
21 Control and Prevention, Atlanta, GA

22 ⁸ St. Luke's Regional Health Care System, Duluth, Minnesota, USA

23 ⁹ University of Miami, Leonard M. Miller School of Medicine, Miami, FL, USA

24 ¹⁰ Kaiser Permanente Northwest Center for Health Research, Portland, Oregon, USA

25 ¹¹ Baylor Scott & White Health and Texas A&M University College of Medicine, Temple,
26 Texas, USA

27 ¹² Rocky Mountain Center for Occupational and Environmental Health, Department of
28 Family and Preventive Medicine, University of Utah Health, Salt Lake City, Utah, USA

29 ¹³ Abt Associates, Rockville, Maryland, USA

30 ¹⁴ Office of the Senior Vice-President for Health Sciences, University of Arizona,
31 Tucson, AZ, USA

32 ¹⁵ BIO5 Institute, University of Arizona, Tucson, AZ, USA

33 ¹⁶ University of Arizona Center on Aging, University of Arizona College of Medicine,
34 Tucson, AZ, USA

35 ¹⁷ Department of Surgery, University of Arizona College of Medicine, Tucson, AZ, USA

36 *These authors contributed equally

37 #These authors contributed equally

- 38 ^Current address: Department of Microbiology and Immunology, Cornell University,
39 Ithaca, NY
- 40 Address correspondence to: deeptab@arizona.edu

Summary:

Vaccine-induced immunity may impact subsequent *de novo* responses to drifted epitopes in SARS-CoV-2 variants, but this has been difficult to quantify due to the challenges in recruiting unvaccinated control groups whose first exposure to SARS-CoV-2 is a primary infection. Through local, statewide, and national SARS-CoV-2 testing programs, we were able to recruit cohorts of individuals who had recovered from either primary or post-vaccination infections by either the Delta or Omicron BA.1 variants. Regardless of variant, we observed greater Spike-specific and neutralizing antibody responses in post-vaccination infections than in those who were infected without prior vaccination. Through analysis of variant-specific memory B cells as markers of *de novo* responses, we observed that Delta and Omicron BA.1 infections led to a marked shift in immunodominance in which some drifted epitopes elicited minimal responses, even in primary infections. Prior immunity through vaccination had a small negative impact on these *de novo* responses, but this did not correlate with cross-reactive memory B cells, arguing against competitive inhibition of naïve B cells. We conclude that dampened *de novo* B cell responses against drifted epitopes are mostly a function of altered immunodominance hierarchies that are apparent even in primary infections, with a more modest contribution from pre-existing immunity, perhaps due to accelerated antigen clearance.

Introduction:

Within a year of the discovery of SARS-CoV-2 as the etiological agent of COVID-19¹, highly effective vaccines were developed and administered. Leading this class were the monovalent mRNA vaccines BNT162b2 and mRNA-1273 encoding the ancestral Spike protein, both of which achieved ~95% efficacies in preventing symptomatic illness^{2,3}. Other vaccine platforms also achieved high efficacies, especially against severe illness and hospitalization^{4–8}. Since the initial results of these clinical trials, however, the protective capacity of these vaccines has declined^{9–12}. This drop in vaccine effectiveness is due to both waning of antibodies and viral evolution and escape from vaccine-induced neutralizing antibodies, which are the best-known correlates of protection^{13,14}. While the known genetic diversity of SARS-CoV-2 was quite modest through most of 2020¹⁵, new variants with enhanced transmissibility and/or neutralizing antibody escape mutations have since emerged and sequentially swept to global dominance^{12,16–24}. As of this writing, the dominant circulating variant is Omicron, which comprises sublineages that contain Spike protein mutations located within most known neutralizing antibody epitopes²⁵. A key issue that will define both protection against infections and the strategy underlying updates to the vaccines is the extent to which pre-existing vaccine-induced immunity protects against heterologous challenges like Omicron.

B cell responses following mRNA COVID-19 vaccination are characterized by exceptionally long-lived germinal center reactions that persist for months while continuously improving the breadth and affinity of antibodies^{26–29}. Cells exiting the germinal center carry affinity-enhancing mutations and can become long-lived antibody-

secreting plasma cells or memory B cells³⁰. Depending on the subset of memory B cell, re-exposures to antigen trigger differentiation to new plasma cells or germinal center reactions^{31–34}. After antigens from infection or vaccine antigens have been cleared, long-lived plasma cells and memory B cells persist to maintain humoral immunity.

While these features protect against homologous SARS-CoV-2 infections, it is more difficult to predict the nature of responses to subsequent heterologous infections or vaccines. Due to their expanded pre-existing numbers and intrinsic signaling and transcriptional differences relative to naive B cells, memory B cells rapidly mount responses that are of greater magnitude than those of naïve primary responses^{35–40} to either initial infection or vaccination. Because of these properties, memory B cells that react to epitopes conserved between the original and secondary challenges could dominate the response to heterologous infections or vaccines^{41–43}. If antigen and T cell help are limiting, memory B cells might then outcompete naive B cells and new primary antibody responses aimed at the new variant-specific epitopes. This phenomenon, known as antigenic imprinting or “original antigenic sin”⁴⁴, can be beneficial if antibodies against the conserved epitopes are protective. However, recall responses to heterologous pathogens can potentially be neutral or even detrimental if antibodies targeting these conserved epitopes are not protective and variant-specific primary responses are competitively inhibited⁴⁵. As an example of the phenomenon, pre-existing common coronavirus-specific memory B cells compose a majority of the early response to SARS-CoV-2, but primary responses to epitopes unique to SARS-CoV-2 are readily observed later^{26,46,47}. Whether common coronavirus immunity is helpful, harmful, or neutral for *de novo* responses to SARS-CoV-2 is unknown.

In influenza infections, antigenic imprinting has been proposed to explain the age-associated differential in morbidity and mortality based on influenza subtype exposure history^{48–51}. The various hemagglutinin (HA) subtypes of influenza A virus fall into one or the other of two phylogenetically distinct HA “groups” (group 1 or group 2). Individuals have the highest antibody titers against influenza strains encountered early in life, and they experience enhanced protection against influenza strains that are within the same HA group as their primary infection strain compared to heterosubtypic infections from the group that is mismatched to their first childhood infection. Previous work has shown that childhood exposure to H1N1 (group 1 hemagglutinin (HA)) affords protection against other group 1 HAs, such as H5N1. The same is true for individuals with group 2 HAs, whereby childhood H3N2 infection affords protection against H7N9. Conversely, individuals with group 1 imprinting experience an increase in mortality when faced with a group 2 influenza virus infection, such as that observed for H7N9 infections^{48,51}.

Though pre-existing immunity can certainly impact primary responses to heterologous antigens, other mechanisms can also limit antibody responses to drifted epitopes. Epitopes that were previously immunodominant for antibody responses do not necessarily remain so once mutated, irrespective of prior immunity⁵². There are several possible mechanistic reasons why not all epitopes are equal for antibody responses. Factors such as naïve antigen-specific B cell precursor frequency and avidity vary greatly across epitopes, which in turn correlate with their relative contribution to the subsequent response^{53–57}. Some epitopes can also be biophysically challenging for antibody binding, such as those sterically blocked by glycan shields or appearing as

non-complex ‘smooth’ surfaces to B cells^{58,59}. Further, epitopes that mimic self-antigens also elicit poor responses due to tolerance mechanisms that remove or hamper B cells from the repertoire that could otherwise respond^{60–63}. Finally, V gene usage during V(D)J recombination that gives rise to B cell receptors is uneven, as some segments are more heavily utilized than others^{64,65}. In turn, this can create ‘holes’ in the repertoire, rendering some epitopes poorly immunogenic⁶⁶. As SARS-CoV-2 variants of concern accumulate mutations in antigenic regions, immunodominance might change in ways that limit responses to drifted epitopes, with or without prior immunity. Thus, it has remained difficult to examine the degree to which infrequent *de novo* variant-specific responses in post-vaccination infections and heterologous boosters are due to changes in immunodominance, antigenic imprinting, or some combination of both^{67–75}.

Antigenic imprinting has remained nearly impossible to quantify directly and instead has predominantly relied on historical epidemiological data to make inferences about biological mechanisms that produce the documented patterns^{48,76,77}. The COVID-19 pandemic presents a unique opportunity to address these questions: it has encompassed adults with known infection histories and monovalent vaccines that induce well characterized B cell responses^{79,81,83,85} and the emergence of antigenically distinct viral variants^{25,87}. Yet, as immunological histories become more complex and with very few immunologically naïve adults remaining⁸², the Omicron BA.1 (BA.1, for short) wave likely represented the final opportunity to recruit robust cohorts of individuals that meet the key experimental and control criteria. Through voluntary saline-gargle PCR testing of University of Arizona students, staff, and faculty as part of COVID mitigation efforts on campus from August 2020 to July 2023; serological testing at 17

University of Arizona-managed sites across the state of Arizona; and two CDC-funded cohorts of essential workers, Arizona Healthcare, Emergency Response, and Other Essential Workers Surveillance (AZ HEROES)⁸⁴ and Research on Epidemiology of SARS-CoV-2 in Essential Response Personnel (RECOVER)⁸⁶, we recruited unvaccinated individuals who had recovered from primary Delta (B.1.617.2 or B.1.617.2-like) or BA.1 (B.1.1.529 or B.1.1.529-like) infections. These cohorts allowed us to characterize the immunodominance hierarchies for both Delta and BA.1 variants and directly compare the specificity of antibody responses in unvaccinated individuals infected by the antigenically drifted viral variants to those generated by post-vaccination infection by Delta or BA.1. In doing so, we were able to quantify the impact of antigenic imprinting on *de novo* responses to drifted epitopes.

Results:

From our voluntary on-campus testing program at the University of Arizona, we recruited 37 participants who had tested positive for SARS-CoV-2 infections between July 1, 2021 and December 1, 2021 despite completion of the primary vaccine series of monovalent BNT162b2 or mRNA-1273 prior to infection (described in detail in Methods section). We also recruited 12 individuals who tested positive during this period but had not received any COVID-19 vaccines. Symptoms reported by participants following infections were similar between primary and post-vaccination infections; none required hospitalization. A slightly larger portion of post-vaccination infections were asymptomatic relative to primary infections (**Figure S1A**), and in general, the duration of symptoms was significantly shorter in this group relative to those who were unvaccinated at the time of infection (**Figure S1B**). All recruited individuals who tested positive by RT-qPCR and had sufficient sequence coverage to assign a lineage had sequences confirmed to be Delta (**Figure S2A**). During this period, the Delta variant represented 100% of PCR+ samples on campus that could be assigned a PANGO-lineage⁸⁷, as determined through viral sequencing of all remnant samples below a Ct value of 35 (**Figure S2B**). We also selected 71 serum samples as part of our statewide antibody testing initiative⁸⁸ from vaccinated participants who had no self-reported prior SARS-CoV-2 infections. This cohort was chosen based on matching for age, sex, and time post-vaccination with our post-vaccination infection group. Characteristics of the cohorts are listed in **Table 1**.

Participants provided blood samples at an average of 75 days (IQR for primary and post-vaccination infections = 45.8 days, 97.3 days; **Table 1**) after testing positive for

SARS-CoV-2 infections and at an average of nine months (IQR for vaccinated only and post-vaccination infections = 56 days, 317 days; **Table 1**) after their last vaccine dose. Using plasma from these samples, we first performed live virus neutralization assays on both an early-pandemic virus representative, (WA-1, from January 2020) or on the antigenically drifted Delta variant. Against both WA-1 and Delta, post-vaccination Delta infections led to significantly higher titers of neutralizing antibodies than both primary infections and vaccinated only controls (**Figure 1A**), indicating a robust recall response.

Elevated neutralizing antibody titers in post-vaccination Delta infections could arise from both memory B cell responses to conserved neutralizing epitopes and primary responses against new variant-specific epitopes. To begin to determine the relative specificities of antibodies following Delta infections, we performed ELISAs to measure the magnitude of the antibody response against Wuhan/Hu1/2019 (hereafter WuHu1) and Delta Spike antigens. WuHu1 was sampled in December 2019 and is the SARS-CoV-2 reference sequence; its Spike amino acid sequence is identical to that of WA-1. We first measured antibodies that bound the receptor binding domain (RBD), as most neutralizing antibodies target this region^{89,90}. Post-vaccination Delta infections led to elevated RBD-binding antibody titers, both against WuHu1 and Delta, relative to vaccination only and primary Delta infection controls (**Figure 1B**), again confirming a robust recall response. As expected, vaccination-only controls showed slightly elevated titers of WuHu1 RBD-binding antibodies relative to Delta RBD antibodies (**Figure 1B, right panel**). Reciprocally, primary Delta infections led to a skewing towards Delta RBD-binding antibodies (**Figure 1B, right panel**). Post-vaccination-Delta infections led to an even ratio of WuHu1:Delta RBD-binding antibodies (**Figure 1B, right panel**),

similar to prior studies⁹¹. Aside from the RBD, neutralizing antibodies can also bind other regions of the S1 domain of Spike^{92–94}. As with RBD, post-vaccination Delta infections led to an even ratio of antibodies that bound WuHu1 and Delta S1 relative to vaccination alone or primary Delta infections (**Figure S3**).

To more directly assess antibody specificities with single cell resolution in post-vaccination Delta infections, memory B cells using WuHu1 S1 and Delta S1 antigen tetramers were quantified by flow cytometry. We focused our analysis on the isotype-switched CD27+ subset (**Figure 2A and Figure S4**), since few Spike-specific cells are observed in other memory B cell subsets⁹⁵. Memory B cells that bound Delta S1 only were observed in both primary infections and in post-vaccination Delta infections, suggesting that in both cases, *de novo* responses aimed at variant-unique epitopes were mounted (**Figure 2A-B**). However, the proportions of these cells in PBMCs were slightly reduced in post-vaccination Delta infections relative to primary Delta infections (**Figure 2B**). Reciprocally, cross-reactive memory B cells that bound both WuHu1 S1 and Delta S1 were elevated in post-vaccination Delta infections relative to primary Delta infections (**Figure 2B**), consistent with a robust recall response and antigenic imprinting, though for a subset of individuals this appears to be more modest. In both primary and post-vaccination Delta infections, memory B cells that bound Delta S1 uniquely were rare relative to cross-reactive cells that bound both WuHu1 and Delta S1 (**Figures 2A-B**). Although these data suggest that pre-existing immunity limits new primary responses, cross-reactive and Delta-specific memory B cells were positively correlated in post-vaccination Delta infections (**Figure 2C**), arguing against a mechanism of competitive inhibition between these two cellular compartments.

The RBD of Delta contains two non-synonymous point mutations that deviate from the vaccine sequence: T478K and L452R. The L452R mutation in particular leads to neutralizing antibody escape^{90,96–98}. To estimate the epitope preferences of serum antibodies further, we produced a Delta RBD protein in which R452 was reverted to L452. Vaccination led to a response that was skewed toward the L452-containing RBD (**Figure 3A**, compare to **Figure 1B, middle panel**), confirming the strong antibody bias and immunodominance of this epitope reported previously⁹⁹. Yet reciprocal skewing to R452-containing RBD was not observed in primary Delta infections, suggesting that a new immunogenic epitope is not created by this mutation (**Figure 3A**). Post-vaccination Delta infections led to a relatively even ratio of antibodies that bound Delta-L452 to those that reacted to Delta-R452 (**Figure 3A**), perhaps due to boosted levels of antibodies that bound other conserved sites on RBD and the T478K epitope. We also produced chimeric WuHu1 S1 proteins in which the Delta N-terminal domain (NTD) supersite mutations (T19R, G142D, E156-, F157-, R158G) were introduced onto a WuHu1 background^{92–94}. Vaccination only controls showed a relatively even distribution of antibodies that bound WuHu1 S1 and Delta NTD-WuHu1 S1 (**Figure 3B** compare to **Figure S3, left panel**). Primary Delta infections, however, were subtly but significantly skewed towards the Delta NTD (**Figure 3B**). Together, these data demonstrate a shifting of immunodominance profiles, even in the absence of prior SARS-CoV-2 immunity.

To more precisely measure clonal shifts in antibody specificities and immunodominance than can be achieved by serological assays, we performed LIBRA-seq using PBMC samples from primary and post-vaccination Delta infections¹⁰⁰.

Streptavidin-phycoerythrin (PE) tetramers were constructed using WuHu1 S1, Delta S1, Delta RBD, Delta RBD-L452, and Delta NTD-WuHu1-S1, as described in **Figures 1, 3** and **S3**, each carrying unique oligonucleotide barcodes. PE-binding memory cells were then enriched and subjected to scRNA/V(D)J-seq. Consistent with our serological data (**Figure 1D**), we observed few memory B cells that bound Delta RBD- and NTD-specific epitopes (**Figure 3C**). A clear preference for Delta-unique epitopes in the NTD relative to the RBD was observed within individuals (**Figure 3D**). Within each group, we did not observe any clear differences in epitope-dependence of somatic mutation frequencies in memory B cells (**Figure S5A-B**). We did, however, observe a greater frequency of somatic mutations in Spike-specific memory B cells in the post-vaccination Delta infection cohort relative to primary Delta infections (**Figure S5C**). Together, these data suggest a marked shift in antibody specificities in primary Delta variant infections relative to WuHu1 Spike. This explains in part why responses to at least some drifted epitopes are not observed, irrespective of prior vaccination.

During the course of this work, the heavily mutated Omicron (BA.1) variant rapidly overtook Delta and swept to global dominance. To define post-vaccination BA.1 responses, we recruited individuals from our voluntary on-campus testing program who had tested positive for SARS-CoV-2 between January 1 and March 31, 2022, with the expectation that primary responses would be robust against this more antigenically distant variant¹⁰¹. All individuals for this study who tested positive by PCR had sequences confirmed to be BA.1 (**Figure S2A**). Individuals with a SARS-CoV-2 infection caused by a Delta variant or other Omicron sublineages were excluded from the study. Viral genome sequencing of all remnant PCR+ samples on campus during

this period below a Ct value of 35 demonstrated that 93.7% of samples that could be assigned a PANGO-lineage^{82,101} were caused by the BA.1 sublineage of Omicron (**Figure S2B**). To obtain controls for this cohort, some of whom had received 3 doses of mRNA vaccines, we also recruited a new group of vaccinated individuals who had never tested positive in our voluntary university testing system and reported no known prior SARS-CoV-2 infections. After testing plasma for nucleocapsid antibodies as a marker of prior infection, samples from 5 individuals with titers well above the mean values seen in verified infections were excluded from further consideration (**Figure S6**). Relative to both primary and post-vaccination Delta infections, post-vaccination BA.1 infections generally led to fewer symptoms such as wet cough (**Figure S1A**) and shorter duration of symptoms (**Figure S1B**).

We were unable to recruit any unvaccinated individuals on campus who had experienced BA.1 infections. However, we were able to obtain serum and, for a subset, PBMC samples from a separate study from the Centers for Disease Control and Prevention HEROES and RECOVER projects^{82,102}, in which 53 individuals met these criteria (**Table 1**). Neutralizing antibody titers were skewed towards WA-1 in individuals who had been vaccinated but not infected (**Figure 4A**). Post-vaccination BA.1 infections led to significantly higher neutralizing antibody titers against BA.1 compared to both vaccinated controls who had not been infected and primary infections (**Figure 4A**), consistent with a memory B cell recall response.

We next examined binding antibody titers against WuHu1 or BA.1 RBD. Post-vaccination BA.1 infections led to increased levels of RBD-binding antibodies, both for WuHu1 and BA.1, relative to the vaccinated only control cohort and primary BA.1

infections (**Figure 4B, left and middle panels**). Vaccination alone led to greater RBD titers against BA.1 than did primary BA.1 infections, despite the many mismatches in sequence (**Figure 4B, middle panel**). As expected, antibodies from vaccinated only individuals were skewed towards WuHu1 relative to BA.1 RBD (**Figure 4B, right panel**). Of the few antibodies induced by primary BA.1 infections, we observed a skewing of specificities towards BA.1 RBD (**Figure 4B, right panel**). Ratios of WuHu1 and BA.1 RBD-binding antibodies in post-vaccination BA.1 infections more closely resembled vaccinated controls than primary BA.1 infections (**Figure 4B, right panel**).

To further evaluate the specificities of antibody responses in post-vaccination BA.1 infections, we again used antigen tetramers to identify RBD-specific memory B cells (**Figures S7 and 5A**). As expected, primary BA.1 infections generated a lower frequency of WuHu1 RBD-specific memory B cells compared to vaccinated controls (**Figure 5B, left panel**). Unexpectedly, BA.1-specific RBD memory B cells were not consistently detectable above background in any experimental group, even primary BA.1 infections (**Figure 5B, middle panel**). These data seem to differ from the modest skewing of the serological response seen above in primary BA.1 infections (**Figure 4B, right panel**), but can potentially be explained by low overall responses and prior studies that observed only partial overlap between memory B and antibody-secreting plasma cell specificities and repertoires^{43,103,104}. Instead, most RBD-specific memory B cells from all cohorts were cross-reactive against WuHu1 and BA.1 RBD (**Figure 5A, 5B, right panel**). Primary BA.1 infections produced numerically fewer cross-reactive RBD memory B cells than did post-vaccination BA.1 infections (**Figure 5B, right panel**).

Given that the overall antibody and memory B cell response to BA.1 RBD was quite modest (**Figures 4B, 5A-B**), we employed tetramers of full-length Spike trimers of WuHu1 and BA.1 Spike to capture a greater breadth of memory B cell specificities than could be observed with RBD tetramers (**Figures 5C**). WuHu1-specific memory B cells were observed in vaccinated controls and post-vaccination BA.1 infections, but not after primary BA.1 infections (**Figures 5D, left panel**). We again failed to consistently observe BA.1-specific memory B cells in any of the groups, including primary BA.1 infections, though a subset of post-vaccination BA.1 infections did appear to generate such cells well above background levels (**Figure 5D, middle panel**). As with RBD, cross-reactive Spike-specific memory cells were significantly elevated in post-vaccination BA.1 infections relative to primary BA.1 infections, but not relative to vaccinated only controls (**Figure 5D, right panel**). Cross-reactive memory B cells composed by far the largest portion of SARS-CoV-2 specific responses within all experimental groups (**Figure S8**).

For a subset of primary BA.1 and post-vaccination BA.1 cohorts, we obtained samples which enabled us to quantify WuHu1, BA.1, and cross-reactive Spike- and RBD- specific memory B cell frequencies before and after BA.1 infection. Irrespective of vaccination status, memory B cells that were either WuHu1- or BA.1-RBD-specific increased in frequency for only a subset of individuals after BA.1 infection (**Figure 6A, left and middle panels**). However, cross-reactive RBD memory B cells consistently and significantly increased after both primary and post-vaccination BA.1 infections (**Figure 6A, right panel**). The frequency of cross-reactive Spike memory B cells also significantly increased after primary BA.1 infections (**Figures 6B, right panel**).

To infer potential mechanisms of antigenic imprinting from these samples, we first correlated pre-infection cross-reactive Spike-specific memory B cells and post-infection BA.1 Spike-specific memory B cells. A negative correlation could indicate detrimental imprinting, whereby pre-existing memory B cells outcompete naïve B cells and inhibit the generation of variant-specific responses. Instead, we observed a slight positive but non-statistically significant correlation between pre-infection cross-reactive Spike-specific memory B cells and post-infection BA.1 Spike-specific memory B cells (**Figure 7A**). Similarly, we observed a non-significant positive correlation between post-infection cross-reactive Spike-specific memory B cells and post-infection BA.1 Spike-specific memory B cells (**Figure 7B**).

Given that these data do not support a mechanism of competitive inhibition of naïve B cells by cross-reactive memory B cells, we explored other mechanisms by which *de novo* responses to drifted epitopes are indirectly suppressed, such as accelerated viral clearance by neutralizing antibodies and/or T cells. We found a negative, but non-statistically significant correlation of *de novo* responses with pre-infection BA.1 neutralizing antibody titers (**Figure 7C**). Similarly, we observed a small and non-significant negative correlation with pre-infection BA.1 Spike-specific T cell numbers and post-infection BA.1 Spike memory B cells (**Figure 7D**). The small sample sizes and variable times of blood sampling prior to infection preclude us from making definitive conclusions about mechanisms driving antigenic imprinting. Nonetheless, the data suggest that neutralizing antibody and/or memory T cell-mediated viral clearance may indirectly underlie suppression of responses to drifted epitopes. This overall impact

369 is quite small relative to the marked changes in antibody immunodominance observed
370 in even primary BA.1 variant infections, irrespective of prior immunity.

Discussion:

Antigenic imprinting is neither inherently beneficial nor detrimental; rather the impact of prior immunity is context-dependent^{104–106}. For example, pre-existing serum antibodies can improve and focus *de novo* responses upon reinfection to only mutated novel epitopes through epitope masking^{105–107}. Similarly, *de novo* responses to drifted epitopes can be improved by pre-existing CD4+ memory T cells in what is classically known as the hapten-carrier effect¹⁰⁸. Alternatively, high affinity memory B cells can competitively inhibit naïve B cells by consuming limited amounts of antigen and T cell help, leading to a suppression of *de novo* antibody responses¹⁰⁹. If these memory B cells target non-protective epitopes, this could in theory leave one worse off than if there were no prior immunity whatsoever^{44,110}. Finally, pre-existing immunity could indirectly suppress new antibody responses to drifted epitopes simply by clearing away virus and antigen before naïve B cells can robustly participate.

Though neutralizing antibody titers were robust following post-vaccination infections, our results demonstrated a small negative impact of prior immunity on *de novo* responses to drifted epitopes. Yet we found no evidence to support a mechanism of competitive inhibition by cross-reactive memory B cells. Though not definitive, our data instead hint at a role for pre-infection neutralizing antibodies and memory T cells, suggesting that antigen clearance is the main mechanism by which *de novo* B cell responses are indirectly suppressed by prior immunity. Indeed, pre-existing neutralizing antibodies likely accelerate viral clearance^{111,112}, and viral and vaccine antigens can potentially also be cleared by T cells or non-neutralizing antibodies via Fc effector functions^{113–115}. Animal studies offer an attractive way to further test mechanisms of

antigenic imprinting on heterologous vaccine and viral infection responses. For example, genetic tracking studies were used to show robust *de novo* responses to Omicron boosters in mice previously vaccinated against the ancestral strain. Yet this required two booster doses, and a small negative impact of prior immunity was observed in inverse proportion to the antigenic distance between the two immunizations¹⁰¹. Similar results have been reported in other mouse studies¹¹⁶. These systems can thus potentially be used to manipulate specific immune parameters and measure their contributions to antigenic imprinting in ways that are not possible in human studies, especially since few immunologically naïve adults remain to serve as controls.

Immunodominance hierarchies can also determine which epitopes are available to be targeted by antibodies, irrespective of prior immunity. Prior studies, confirmed in our experiments, showed that a large portion of COVID-19 vaccine-induced antibodies are aimed at the L452 class 3 epitope¹¹⁷. Yet in the post-vaccination Delta cohort, we observed few antibodies directed at the epitope containing the L452R mutation. Under the assumption that one immunodominant epitope was being mutated to another, one might have concluded that the absence of R452-specific antibodies could be explained by antigenic imprinting. Yet by including a primary infection cohort, we observed that the Delta variant intrinsically did not elicit detectable antibody responses against the R452 epitope, even with no prior SARS-CoV-2 exposures, consistent with an independent study¹⁰⁰. We can instead conclude that Delta shifts antibody immunodominance hierarchies to instead focus more on epitopes located in the NTD. These types of shifts in immunodominance preempt any considerations of the impact of antigenic imprinting.

The basis and mechanisms of these shifts for SARS-CoV-2 clearly needs more investigation to determine whether and how best to overcome them.

This study spanned a period from the Delta wave through the more antigenically distinct BA.1 Omicron wave. A central expectation of antigenic imprinting is that the extent to which prior immunity interferes with *de novo* responses should decrease as antigenic distance increases¹⁰¹. We used the Delta and BA.1 variants to test this expectation in SARS-CoV-2 and to understand the impacts of antigenic distance on antigenic imprinting. Despite our prediction, we observe even less of a variant specific response in post-vaccination BA.1 infections compared to post-vaccination Delta infections. Much of this can be explained by shifts in immunodominance in which even primary BA.1 infections elicited few memory B cell responses to drifted epitopes. Yet longitudinal sampling during BA.1 infections has also shown that viral titers do not reach the peak levels observed in Delta infections¹¹⁸, suggesting that immune responses to drifted epitopes occur in proportion to need and antigen availability.

Disclosures: The findings and conclusions in this report are those of the authors and do not necessarily represent the official position of the Centers for Disease Control and Prevention.

Acknowledgements: This work was supported by NIH grants R01AI099108 and R01AI129945 (D.B.) and a research grant from the Arizona Board of Regents (M.W. and D.B.). This project has been funded in part with Federal funds from the National Institute of Allergy and Infectious Diseases, National Institutes of Health, Department of Health and Human Services, under Contract No. 75N93021C00015 (M.W.) The HEROES-RECOVER cohort is supported by the National Center for Immunization and Respiratory Diseases and the Centers for Disease Control and Prevention (contracts 75D30120R68013 to Marshfield Clinic Research Institute, 75D30120C08379 to the University of Arizona, and 75D30120C08150 to Abt Associates).

Declaration of Interests: Sana Biotechnology has licensed intellectual property of D.B. and Washington University in St. Louis. Gilead Sciences has licensed intellectual property of D.B. and Stanford University. Clade Therapeutics has licensed intellectual property of D.B. and University of Arizona. D.B. is a co-founder of Clade Therapeutics. D.B. served on an advisory panel for GlaxoSmithKline. B.J.L. has a financial interest in Cofactor Genomics, Inc. and Iron Horse Dx. Geneticure Inc. has licensed intellectual property of R.S. and R.S is a co-founder of Geneticure Inc. M.W. has received consulting fees from GLG on SARS-CoV-2 and the COVID-19 pandemic.

Methods:

Participant selection

All human studies conducted at The University of Arizona were approved by the Institutional Review Board for the Human Subjects Protection Program[†]. Individuals who had participated in the voluntary on-campus saline gargle testing program and had either never tested positive or had tested positive during the Delta or BA.1 waves were contacted by email by the program administrators (not the authors on this study) about willingness to participate in this research study. Participants were provided a link to an eligibility questionnaire and, once eligibility (no immunosuppressive therapy in the last 5 years and HIV negative) was confirmed, additional demographic questions and a link to schedule an appointment for blood draws. Written consent was obtained through an electronic form. All blood draws were performed at the Clinical and Translational Sciences Center at The University of Arizona. Additional primary and post-vaccination BA.1 infection samples were acquired from the CDC HEROES-RECOVERS^{††} cohort^{82,84}. This study was reviewed by CDC and approved by the institutional review boards at participating sites or under a reliance agreement with Abt Associates institutional review board and was conducted consistent with applicable federal law and CDC policy under 45 C.F.R. part 46, 21 C.F.R. part 56, 42 U.S.C. Sect. 241(d), 5 U.S.C. Sect. 552a, 44 U.S.C. Sect. 3501 et seq. Methods for the HEROES-RECOVER Cohorts have been published previously¹¹⁸. In summary, cohorts consisted of health care personnel, first responders, and other essential and frontline workers in eight U.S. locations across six states. Participants collected weekly nasal

swabs which were tested for SARS-CoV-2 viral material by RT-qPCR and additional swabs were collected and screened upon the onset of any COVID-19–like illness symptoms. In addition, blood draws were collected at enrollment, then approximately every 3 months and after immune modifying events such as vaccination or infection. Vaccination was documented by self-report and verified by vaccine cards or electronic medical records or state immunization registries. HEROES-RECOVER participants were selected based on testing positive for SARS-CoV-2 during Delta or BA.1 waves and having completed a blood draw after infection.

Saline Gargle PCR testing for SARS-CoV-2

As part of Test All, Test Smart, the University of Arizona’s voluntary campus-wide testing program, University staff, faculty and students had access to SARS-CoV-2 rRT-PCR tests from August 2020 – July 2023. At testing and collection sites throughout campus, individuals were given 5 mL of 0.9 % sterile saline (AddiPak 5 mL sterile saline single use tubes, Teleflex, LLC) and guided to complete three rounds of a 5-second swish followed by 10 seconds of gargling (adapted from Goldfarb et al.¹¹⁹). Samples were deposited into collection tubes and then screened for SARS-CoV-2 by rRT-PCR.

PBMC and plasma preparation

Twenty milliliters of blood was collected by venipuncture in heparinized Vacutainer tubes (BD). For PBMCs, 15ml of Ficoll-Paque PLUS (Thermo Fisher Scientific) was added to 50-ml Leucosep tubes (Greiner) and spun for 1min at 1,000g to transfer the density gradient below the filter. Twenty milliliters of blood from the heparinized tubes

was then poured into the top of the Leucosep tube and spun at 1,000g for 10min at room temperature with the brake off. The top plasma layer was carefully collected and frozen at -20°C , and the remaining supernatant containing PBMCs above the filter was poured into a new 50-ml conical tube containing 10mL of PBS and spun at 250g for 10min. Cell pellets were resuspended in RPMI media containing 10% FCS and counted on a Vi-Cell XR (Beckman Coulter). Cells were diluted to a concentration of 2×10^7 cells per mL in RPMI media containing 10% FCS. An equal volume of 80% FCS + 20% dimethyl sulfoxide was added dropwise and inverted once to mix. Suspensions were distributed at 1ml per cryovial and frozen overnight at -80°C in Mr. Frosty freezing chambers (Nalgene). Vials were then transferred to storage in liquid nitrogen.

ELISA and quantification of antibody titers

Serological assays were performed as previously described⁸⁸. WuHu1 RBD (cat. no. SPD-C52H3), WuHu1 S1subdomain of the SARS-CoV-2 S glycoprotein (cat. no. S1N-C52H3), WuHu1 Spike (cat. no. SPN-C52H9), Delta RBD (cat. no. SPD-C52Hh), Delta S1 subdomain (cat. no. S1N-C52Hu), Omicron (BA.1) RBD (cat. no. SPD-C522e), Omicron (BA.1) Spike (cat. no. SPN-C52Hz) and Nucleocapsid (cat. no. NUN-C5227) were purchased from Acro Biosystems. Chimeric proteins (Delta RBD-L452 and Delta NTD-WuHu1 S1) were custom synthesized by GenScript. To obtain titers and single-dilution OD450 values, antigens were immobilized on high-adsorbency 384-well plates at 5 ng mL^{-1} . Plates were blocked with 1% non-fat dehydrated milk extract (Santa Cruz Biotechnology, sc-2325) in sterile PBS (Thermo Fisher Scientific HyClone PBS,

SH2035) for 1 h, washed with PBS containing 0.05% Tween-20 and overlaid for 60 min with either a single 1:60 dilution or five serial 1:3 dilutions beginning at a 1:60 dilution of serum. Plates were then washed and incubated for 1 h in 1% PBS and milk containing anti-human Pan-Ig HRP-conjugated antibody (Jackson ImmunoResearch, 109-035-064) at a concentration of 1:2,000 for 1 h. Plates were washed with PBS-Tween solution followed by PBS wash. To develop, plates were incubated in tetramethylbenzidine (Fisher Scientific) before quenching with 2 N H₂SO₄. Plates were read for 450-nm absorbance on CLARIOstar Plus from BMG Labtech. All samples were also read at 630 nm to detect any incomplete quenching. Any samples above background 630-nm values were re-run. Area under the curve (AUC) values were calculated in GraphPad Prism (v9).

Virus neutralization assays

All live virus assays were performed at Biosafety Level 3 and were approved by the University of Arizona Institutional Biosafety Committee. SARS-CoV-2, isolate USA-WA1/2020, was deposited by Dr Natalie J. Thornburg at the Centers for Disease Control and Prevention and obtained from the World Reference Center for Emerging Viruses and Arboviruses. Stocks of WA1/2020 SARS-CoV-2 were generated as a single passage from received stock vial on mycoplasma-negative Vero cells (ATCC CCL-81). B.1.617.2 (Delta) was received from WRCEVA, strain designation GNL-1205. B.1.1.529 (Omicron) originated from a nasopharyngeal swab collected at the University of Arizona. It was passaged once on Calu-3 cells and then once on Vero cells to generate a master

stock. Viral PANGO-lineage, BA.1.1¹¹⁹, was confirmed by Illumina sequencing (EPI_ISL_17886211) of the master stock.

Supernatant and cell lysate were combined, subjected to a single freeze–thaw and then centrifuged at 1,800g for 10min to remove cell debris. For PRNTs for SARS-CoV-2, Vero cells (ATCC, CCL-81) were plated in 96-well tissue culture plates and grown overnight. Vero cells were confirmed by PCR to be free of mycoplasma using the Universal Mycoplasma Detection Kit (ATCC). Serial dilutions of serum samples were performed in duplicate and incubated with 100 plaque-forming units of SARS-CoV-2 for 1h at 37 °C. Plasma/serum dilutions plus virus were transferred to the cell plates and incubated for 2h at 37 °C in 5% CO₂ and then overlaid with 1% methylcellulose. After 72h, plates were fixed with 10% neutral buffered formalin for 30min and stained with 1% crystal violet. Plaques were imaged using an ImmunoSpot Versa plate reader. The most dilute serum concentration that led to ten or fewer plaques was designated as the PRNT₉₀ titer. Input PFU for each experiment was confirmed by plaque assay.

Flow cytometry

One milliliter of pre-warmed FBS was added to a frozen cryovial of 10⁷ PBMCs, which was rapidly thawed in a 37°C water bath. Samples were poured into 15 mL conical tubes containing 5 mL of pre-warmed RPMI with 5% FBS and 1% anti/anti. Tubes were spun at 250g for 5 min at room temperature.

Delta

Supernatants were removed and cell pellets were resuspended in 200 µL of staining buffer containing 1 µL each of anti-CD38-APC (BioLegend, clone HIT2), anti-CD13-PE-

Cy7 (BioLegend, clone WM15), anti-CD21-PE-Dazzle (BioLegend, clone Bu32), anti-CD19-APC-eFluor-780 (Invitrogen, clone HIB19), anti-IgD-PerCP-Cy5.5 (Biolegend, clone IA6-2), anti-IgM-FITC (Biolegend, clone MHM-88), anti-CD27-BV510 (Biolegend, clone M-T271), anti-CD11c-Alexa700 (BioLegend, clone Bu15). Staining buffer also contained Delta-S1-PE and S1-BV421 tetramers.

BA.1

Supernatants were removed and cell pellets were resuspended in 200 μ L of staining buffer containing 1 μ L each of anti-CD38-BV421 (BioLegend, clone HB-7), anti-CD13-PE-Dazzle 594 (BioLegend, clone WM15), anti-CD21-PerCP Cy 5.5 (BioLegend, clone Bu32), anti-CD19-APC-eFluor-780 (Invitrogen, clone HIB19), anti-IgD-BV510 (Biolegend, clone 11-26c.2a), anti-IgM-FITC (Biolegend, clone MHM-88), anti-CD27-PE Cy 7 (Biolegend, clone M-T271), anti-CD11c-Alexa700 (BioLegend, clone Bu15). Cells were stained with live-dead marker, Zombie Yellow (BioLegend) according to manufacturer's recommendations. Staining buffer also contained BA.1-Spike-PE and Spike-Alexa Fluor 647 tetramers.

Antibodies were validated by the manufacturer on human PBMCs. Tetramer reagents were assembled by mixing 100 μ g ml⁻¹ of C-terminal AviTagged S1, Delta S1, WuHu1 Spike, or BA.1 Spike (ACROBiosystems) with 100 μ g ml⁻¹ of streptavidin-PE(BioLegend), streptavidin-BV421 (BioLegend), or streptavidin-Alexa Fluor 647 (BioLegend), respectively, at a 6:1 molar ratio for S1 or 4:1 molar ratio for Spike, in which $\frac{1}{5}$ of the final volume of streptavidin was added every 10 min. S1 and Spike tetramers were validated by staining Lenti-X 293T cells(Takara Bio) as a negative control or 293T-

hACE2-expressing cells (BEI Resources, NR-52511) as a positive control. Lenti-X 293T cells were confirmed to be free of mycoplasma; 293T-hACE2 cells were maintained in media containing 1% pen/strep to minimize chances of contamination. PBMC samples were stained for at least 20 minutes, washed and filtered through 70- μ m nylon mesh. Data were analyzed on either a BD LSR2 (tetramer validation only), a Fortessa cytometer (Delta), or BD Cytex Aurora (BA.1). Data were analyzed using FlowJo software.

Flow cytometry and Fluorescence Activated Cell Sorting

One milliliter of pre-warmed FBS was added to a frozen cryovial of PBMCs and thawed by pipetting. Samples were added to 15 mL conical tubes containing 10 mL of pre-warmed RPMI with 20% FBS and 1% anti/anti. Tubes were spun at 1200 RPM for 5 minutes at room temperature. Supernatants were removed and cell pellets were resuspended in 200 μ L of staining buffer contained 1 μ L each of anti-CD19-BV421(Biolegend, clone HIB19), anti-CD27-FITC(Biolegend, clone O323), anti-CD13-PE-Cy-7(Biolegend, clone WM15), anti-IgD-APC-Cy-7(Biolegend, clone IA6-2). Staining buffer also contained either 5 or 2 LIBRA-Seq tetramers: S1-PE(Biolegend, TotalSeq-C0951_PE), Delta S1-PE(Biolegend, TotalSeq-C0952_PE), Delta NTD/S1-PE(Biolegend, TotalSeq-C0953_PE), Delta RBD/L452(Biolegend, TotalSeq-C0954_PE), and Delta RBD-PE(Biolegend, TotalSeq-C0955_PE). Biotinylated tetramer reagents were assembled by mixing 100 μ g ml⁻¹ of C-terminal AviTagged S1 (ACROBiosystems), Delta S1 (ACROBiosystems), Delta NTD/S1 (GenScript), Delta RBD/L452 (Genscript), or Delta RBD (ACROBiosystems) with 100 μ g ml⁻¹ of

streptavidin-TotalSeq-C-PE (BioLegend) at a 6:1 molar ratio in which $\frac{1}{5}$ of the final volume of streptavidin was added every 10 min. Tetramers were validated by staining Lenti-X 293T cells (Takara Bio) as a negative control or 293T-hACE2-expressing cells (BEI Resources, NR-52511) as a positive control. Lenti-X 293T cells were confirmed to be free of mycoplasma; 293T-hACE2 cells were maintained in media containing 1% pen/strep to minimize chances of contamination. Additionally, TotalSeq-C anti-human Hashtag antibodies (Biolegend, TotalSeq™-C0251-10) were added to individual samples and pooled after staining and washing. PBMCs were stained in the dark for 30 minutes at 4°C, washed, pooled and filtered through a 35 µm strainer (Fisher Scientific). SARS-CoV-2 specific memory B cells (CD19+IgD-IgM-CD27+) as well as non-antigen specific memory B cells were sorted using a FACS Aria II.

Single-cell RNA sequencing and analysis

Cells were prepared and processed according to the 10X Genomics Single Cell 5' Dual Index protocol with Feature Barcoding Technology for Cell Surface Protein and Immune Receptor Mapping kit (10X Genomics). Reads were processed and aligned using the 10X Cell Ranger multi pipeline to GRCh38 gex and vdj reference genomes (10X Genomics). Each sample feature barcode matrix was loaded into R and analyzed utilizing the Seurat package for gene expression, vdj and antibody capture analysis¹²⁰. Cell processing was conducted as previously described¹⁰⁰. Data are available at NCBI GEO accession number GSE242775.

ELISpot Assay

Cryopreserved PBMC (5×10^6 /sample) were thawed in prewarmed RPMI-1640 media supplemented with L-glutamine + 10% FCS and 300ug DNase. Thawed PBMCs were rested overnight at 37 °C in X-VIVO™-15 Medium (Lonza) supplemented with 5% human-AB serum. Cells were stimulated with ~1 nmol of peptide pool corresponding to spike of Omicron (B.1.1.529) variant (16-mer peptide pools, overlapping by 10 amino acids (21st century Biochemicals Inc.) on pre-coated human IFN- γ ELISpot plates (Mabtech, Inc.) and developed after 18 hours according to manufacturer instructions. Spots were imaged and counted using Iris FLUOROsport reader (Mabtech).

Statistical methods

All analyses are listed in the figure legends and were performed in GraphPad Prism 9 and/or the R programming language (v4.0.5).

Footnotes

[†] See 45 C.F.R. part 46; 21 C.F.R. part 56

^{††} This study was reviewed by CDC and approved by the institutional review boards at participating sites or under a reliance agreement with Abt Associates institutional review board and was conducted consistent with applicable federal law and CDC policy under 45 C.F.R. part 46, 21 C.F.R. part 56, 42 U.S.C. Sect. 241(d), 5 U.S.C. Sect. 552a, 44 U.S.C. Sect. 3501 et seq.

References

1. Novel 2019 coronavirus genome (2020). Virological. <https://virological.org/t/novel-2019-coronavirus-genome/319>.
2. Baden, L.R., El Sahly, H.M., Essink, B., Kotloff, K., Frey, S., Novak, R., Diemert, D., Spector, S.A., Roupheal, N., Creech, C.B., et al. (2021). Efficacy and safety of the mRNA-1273 SARS-CoV-2 vaccine. *N. Engl. J. Med.* 384, 403–416. 10.1056/NEJMoa2035389.
3. Polack, F.P., Thomas, S.J., Kitchin, N., Absalon, J., Gurtman, A., Lockhart, S., Perez, J.L., Pérez Marc, G., Moreira, E.D., Zerbini, C., et al. (2020). Safety and Efficacy of the BNT162b2 mRNA Covid-19 Vaccine. *N. Engl. J. Med.* 383, 2603–2615. 10.1056/NEJMoa2034577.
4. Sadoff, J., Gray, G., Vandebosch, A., Cárdenas, V., Shukarev, G., Grinsztejn, B., Goepfert, P.A., Truyers, C., Fennema, H., Spiessens, B., et al. (2021). Safety and efficacy of single-dose Ad26.COV2.S vaccine against Covid-19. *N. Engl. J. Med.* 384, 2187–2201. 10.1056/NEJMoa2101544.
5. Tanriover, M.D., Doğanay, H.L., Akova, M., Güner, H.R., Azap, A., Akhan, S., Köse, Ş., Erdinç, F.Ş., Akalın, E.H., Tabak, Ö.F., et al. (2021). Efficacy and safety of an inactivated whole-virion SARS-CoV-2 vaccine (CoronaVac): interim results of a double-blind, randomised, placebo-controlled, phase 3 trial in Turkey. *Lancet* 398, 213–222. 10.1016/S0140-6736(21)01429-X.

6. Heath, P.T., Galiza, E.P., Baxter, D.N., Boffito, M., Browne, D., Burns, F.,
Chadwick, D.R., Clark, R., Cosgrove, C., Galloway, J., et al. (2021). Safety and
efficacy of NVX-CoV2373 covid-19 vaccine. *N. Engl. J. Med.* 385, 1172–1183.
10.1056/NEJMoa2107659.
7. Voysey, M., Clemens, S.A.C., Madhi, S.A., Weckx, L.Y., Folegatti, P.M., Aley, P.K.,
Angus, B., Baillie, V.L., Barnabas, S.L., Bhorat, Q.E., et al. (2021). Safety and
efficacy of the ChAdOx1 nCoV-19 vaccine (AZD1222) against SARS-CoV-2: an
interim analysis of four randomised controlled trials in Brazil, South Africa, and the
UK. *Lancet* 397, 99–111. 10.1016/S0140-6736(20)32661-1.
8. Xia, S., Zhang, Y., Wang, Y., Wang, H., Yang, Y., Gao, G.F., Tan, W., Wu, G., Xu,
M., Lou, Z., et al. (2021). Safety and immunogenicity of an inactivated SARS-CoV-2
vaccine, BBIBP-CorV: a randomised, double-blind, placebo-controlled, phase 1/2
trial. *Lancet Infect. Dis.* 21, 39–51. 10.1016/S1473-3099(20)30831-8.
9. Pouwels, K.B., Pritchard, E., Matthews, P.C., Stoesser, N., Eyre, D.W., Vihta, K.-D.,
House, T., Hay, J., Bell, J.I., Newton, J.N., et al. (2021). Effect of Delta variant on
viral burden and vaccine effectiveness against new SARS-CoV-2 infections in the
UK. *Nat. Med.* 27, 2127–2135. 10.1038/s41591-021-01548-7.
10. Chen, J., Wang, R., Gilby, N.B., and Wei, G.-W. (2022). Omicron variant
(B.1.1.529): Infectivity, vaccine breakthrough, and antibody resistance. *J. Chem. Inf.*
Model. 62, 412–422. 10.1021/acs.jcim.1c01451.

11. Tao, K., Tzou, P.L., Nouhin, J., Gupta, R.K., de Oliveira, T., Kosakovsky Pond, S.L., Fera, D., and Shafer, R.W. (2021). The biological and clinical significance of emerging SARS-CoV-2 variants. *Nat. Rev. Genet.*, 1–17. 10.1038/s41576-021-00408-x.
12. Dejnirattisai, W., Huo, J., Zhou, D., Zahradník, J., Supasa, P., Liu, C., Duyvesteyn, H.M.E., Ginn, H.M., Mentzer, A.J., Tuekprakhon, A., et al. (2022). SARS-CoV-2 Omicron-B.1.1.529 leads to widespread escape from neutralizing antibody responses. *Cell*. 10.1016/j.cell.2021.12.046.
13. Gilbert, P.B., Montefiori, D.C., McDermott, A.B., Fong, Y., Benkeser, D., Deng, W., Zhou, H., Houchens, C.R., Martins, K., Jayashankar, L., et al. (2022). Immune correlates analysis of the mRNA-1273 COVID-19 vaccine efficacy clinical trial. *Science* 375, 43–50. 10.1126/science.abm3425.
14. Khoury, D.S., Cromer, D., Reynaldi, A., Schlub, T.E., Wheatley, A.K., Juno, J.A., Subbarao, K., Kent, S.J., Triccas, J.A., and Davenport, M.P. (2021). Neutralizing antibody levels are highly predictive of immune protection from symptomatic SARS-CoV-2 infection. *Nat. Med.* 27, 1205–1211. 10.1038/s41591-021-01377-8.
15. Rausch, J.W., Capoferri, A.A., Katusiime, M.G., Patro, S.C., and Kearney, M.F. (2020). Low genetic diversity may be an Achilles heel of SARS-CoV-2. *Proc. Natl. Acad. Sci. U. S. A.* 117, 24614–24616. 10.1073/pnas.2017726117.
16. Volz, E. (2023). Fitness, growth and transmissibility of SARS-CoV-2 genetic variants. *Nat. Rev. Genet.*, 1–11. 10.1038/s41576-023-00610-z.

17. Wiegand, T., Nemudryi, A., Nemudraia, A., McVey, A., Little, A., Taylor, D.N., Walk, S.T., and Wiedenheft, B. (2022). The Rise and Fall of SARS-CoV-2 Variants and Ongoing Diversification of Omicron. *Viruses* 14, 2009. 10.3390/v14092009.
18. Hill, V., Du Plessis, L., Peacock, T.P., Aggarwal, D., Colquhoun, R., Carabelli, A.M., Ellaby, N., Gallagher, E., Groves, N., Jackson, B., et al. (2022). The origins and molecular evolution of SARS-CoV-2 lineage B.1.1.7 in the UK. *Virus Evol.* 8, veac080. 10.1093/ve/veac080.
19. Cao, Y., Song, W., Wang, L., Liu, P., Yue, C., Jian, F., Yu, Y., Yisimayi, A., Wang, P., Wang, Y., et al. (2022). Characterization of the enhanced infectivity and antibody evasion of Omicron BA.2.75. *Cell Host Microbe* 30, 1527-1539.e5. 10.1016/j.chom.2022.09.018.
20. Volz, E., Mishra, S., Chand, M., Barrett, J.C., Johnson, R., Geidelberg, L., Hinsley, W.R., Laydon, D.J., Dabrera, G., O'Toole, Á., et al. (2021). Assessing transmissibility of SARS-CoV-2 lineage B.1.1.7 in England. *Nature* 593, 266–269. 10.1038/s41586-021-03470-x.
21. Cherian, S., Potdar, V., Jadhav, S., Yadav, P., Gupta, N., Das, M., Rakshit, P., Singh, S., Abraham, P., Panda, S., et al. (2021). Convergent evolution of SARS-CoV-2 spike mutations, L452R, E484Q and P681R, in the second wave of COVID-19 in Maharashtra, India. *bioRxiv*, 2021.04.22.440932. 10.1101/2021.04.22.440932.
22. Cheng, Y.-W., Chao, T.-L., Li, C.-L., Wang, S.-H., Kao, H.-C., Tsai, Y.-M., Wang, H.-Y., Hsieh, C.-L., Lin, Y.-Y., Chen, P.-J., et al. (2021). D614G Substitution of

SARS-CoV-2 Spike Protein Increases Syncytium Formation and Virus Titer via Enhanced Furin-Mediated Spike Cleavage. MBio, e0058721. 10.1128/mBio.00587-21.

23. McCallum, M., Bassi, J., De Marco, A., Chen, A., Walls, A.C., Di Iulio, J., Tortorici, M.A., Navarro, M.-J., Silacci-Fregni, C., Saliba, C., et al. (2021). SARS-CoV-2 immune evasion by the B.1.427/B.1.429 variant of concern. Science. 10.1126/science.abi7994.

24. Imai, M., Halfmann, P.J., Yamayoshi, S., Iwatsuki-Horimoto, K., Chiba, S., Watanabe, T., Nakajima, N., Ito, M., Kuroda, M., Kiso, M., et al. (2021). Characterization of a new SARS-CoV-2 variant that emerged in Brazil. PNAS. 10.1073/pnas.2106535118/-/DCSupplemental.

25. Viana, R., Moyo, S., Amoako, D.G., Tegally, H., Scheepers, C., Althaus, C.L., Anyaneji, U.J., Bester, P.A., Boni, M.F., Chand, M., et al. (2022). Rapid epidemic expansion of the SARS-CoV-2 Omicron variant in southern Africa. Nature 603, 679–686. 10.1038/s41586-022-04411-y.

26. Sokal, A., Chappert, P., Barba-Spaeth, G., Roeser, A., Fourati, S., Azzaoui, I., Vandenberghe, A., Fernandez, I., Meola, A., Bouvier-Alias, M., et al. (2021). Maturation and persistence of the anti-SARS-CoV-2 memory B cell response. Cell 184, 1201-1213.e14. 10.1016/j.cell.2021.01.050.

27. Muecksch, F., Weisblum, Y., Barnes, C.O., Schmidt, F., Schaefer-Babajew, D., Wang, Z., C Lorenzi, J.C., Flyak, A.I., DeLaitch, A.T., Huey-Tubman, K.E., et al.

(2021). Affinity maturation of SARS-CoV-2 neutralizing antibodies confers potency, breadth, and resilience to viral escape mutations. *Immunity*. 10.1016/j.immuni.2021.07.008.

28. Turner, J.S., O'Halloran, J.A., Kalaidina, E., Kim, W., Schmitz, A.J., Zhou, J.Q., Lei, T., Thapa, M., Chen, R.E., Case, J.B., et al. (2021). SARS-CoV-2 mRNA vaccines induce persistent human germinal centre responses. *Nature*. 10.1038/s41586-021-03738-2.

29. Kim, W., Zhou, J.Q., Horvath, S.C., Schmitz, A.J., Sturtz, A.J., Lei, T., Liu, Z., Kalaidina, E., Thapa, M., Alsoussi, W.B., et al. (2022). Germinal centre-driven maturation of B cell response to mRNA vaccination. *Nature*, 1–8. 10.1038/s41586-022-04527-1.

30. Victora, G.D., and Nussenzweig, M.C. (2022). Germinal centers. *Annu. Rev. Immunol.* 40, 413–442. 10.1146/annurev-immunol-120419-022408.

31. Seifert, M., Przekopowicz, M., Taudien, S., Lollies, A., Ronge, V., Drees, B., Lindemann, M., Hillen, U., Engler, H., Singer, B.B., et al. (2015). Functional capacities of human IgM memory B cells in early inflammatory responses and secondary germinal center reactions. *Proc. Natl. Acad. Sci. U. S. A.* 112, E546-55. 10.1073/pnas.1416276112.

32. Dogan, I., Bertocci, B., Vilmont, V., Delbos, F., Mégret, J., Storck, S., Reynaud, C.-A., and Weill, J.-C. (2009). Multiple layers of B cell memory with different effector functions. *Nat. Immunol.* 10, 1292–1299. 10.1038/ni.1814.

- 785 33. Pape, K.A., Taylor, J.J., Maul, R.W., Gearhart, P.J., and Jenkins, M.K. (2011).
786 Different B cell populations mediate early and late memory during an endogenous
787 immune response. *Science* 331, 1203–1207. 10.1126/science.1201730.
- 788 34. Zuccarino-Catania, G.V., Sadanand, S., Weisel, F.J., Tomayko, M.M., Meng, H.,
789 Kleinstein, S.H., Good-Jacobson, K.L., and Shlomchik, M.J. (2014). CD80 and PD-
790 L2 define functionally distinct memory B cell subsets that are independent of
791 antibody isotype. *Nat. Immunol.* 15, 631–637. 10.1038/ni.2914.
- 792 35. Horikawa, K., Martin, S.W., Pogue, S.L., Silver, K., Peng, K., Takatsu, K., and
793 Goodnow, C.C. (2007). Enhancement and suppression of signaling by the
794 conserved tail of IgG memory-type B cell antigen receptors. *J. Exp. Med.* 204, 759–
795 769. 10.1084/jem.20061923.
- 796 36. Waisman, A., Kraus, M., Seagal, J., Ghosh, S., Melamed, D., Song, J., Sasaki, Y.,
797 Classen, S., Lutz, C., Brombacher, F., et al. (2007). IgG1 B cell receptor signaling is
798 inhibited by CD22 and promotes the development of B cells whose survival is less
799 dependent on Ig alpha/beta. *J. Exp. Med.* 204, 747–758. 10.1084/jem.20062024.
- 800 37. Engels, N., König, L.M., Heemann, C., Lutz, J., Tsubata, T., Griep, S., Schrader, V.,
801 and Wienands, J. (2009). Recruitment of the cytoplasmic adaptor Grb2 to surface
802 IgG and IgE provides antigen receptor-intrinsic costimulation to class-switched B
803 cells. *Nat. Immunol.* 10, 1018–1025. 10.1038/ni.1764.
- 804 38. Kometani, K., Nakagawa, R., Shinnakasu, R., Kaji, T., Rybouchkin, A., Moriyama,
805 S., Furukawa, K., Koseki, H., Takemori, T., and Kurosaki, T. (2013). Repression of

806 the transcription factor Bach2 contributes to predisposition of IgG1 memory B cells
807 toward plasma cell differentiation. *Immunity* 39, 136–147.
808 10.1016/j.immuni.2013.06.011.

809 39. Bhattacharya, D., Cheah, M.T., Franco, C.B., Hosen, N., Pin, C.L., Sha, W.C., and
810 Weissman, I.L. (2007). Transcriptional profiling of antigen-dependent murine B cell
811 differentiation and memory formation. *J. Immunol.* 179, 6808–6819.
812 10.4049/jimmunol.179.10.6808.

813 40. Tomayko, M.M., Anderson, S.M., Brayton, C.E., Sadanand, S., Steinel, N.C.,
814 Behrens, T.W., and Shlomchik, M.J. (2008). Systematic comparison of gene
815 expression between murine memory and naive B cells demonstrates that memory B
816 cells have unique signaling capabilities. *J. Immunol.* 181, 27–38.
817 10.4049/jimmunol.181.1.27.

818 41. Wong, R., Belk, J.A., Govero, J., Uhrlaub, J.L., Reinartz, D., Zhao, H., Errico, J.M.,
819 D’Souza, L., Ripberger, T.J., Nikolich-Zugich, J., et al. (2020). Affinity-Restricted
820 Memory B Cells Dominate Recall Responses to Heterologous Flaviviruses.
821 *Immunity* 53, 1078-1094.e7. 10.1016/j.immuni.2020.09.001.

822 42. Mesin, L., Schiepers, A., Ersching, J., Barbulescu, A., Cavazzoni, C.B., Angelini, A.,
823 Okada, T., Kurosaki, T., and Victora, G.D. (2020). Restricted clonality and limited
824 germinal center reentry characterize memory B cell reactivation by boosting. *Cell*
825 180, 92-106.e11. 10.1016/j.cell.2019.11.032.

- 826 43. Purtha, W.E., Tedder, T.F., Johnson, S., Bhattacharya, D., and Diamond, M.S.
827 (2011). Memory B cells, but not long-lived plasma cells, possess antigen
828 specificities for viral escape mutants. *J. Exp. Med.* *208*, 2599–2606.
829 10.1084/jem.20110740.
- 830 44. Francis, T. (1960). On the Doctrine of Original Antigenic Sin. *Proc. Am. Philos. Soc.*
831 *104*, 572–578.
- 832 45. Worobey, M., Plotkin, S., and Hensley, S.E. (2020). Influenza Vaccines Delivered in
833 Early Childhood Could Turn Antigenic Sin into Antigenic Blessings. *Cold Spring*
834 *Harb. Perspect. Med.* *10*. 10.1101/cshperspect.a038471.
- 835 46. Anderson, E.M., Li, S.H., Awofolaju, M., Eilola, T., Goodwin, E., Bolton, M.J.,
836 Gouma, S., Manzoni, T.B., Hicks, P., Goel, R.R., et al. (2022). SARS-CoV-2
837 infections elicit higher levels of original antigenic sin antibodies compared with
838 SARS-CoV-2 mRNA vaccinations. *Cell Rep.* *41*, 111496.
839 10.1016/j.celrep.2022.111496.
- 840 47. Amanat, F., Thapa, M., Lei, T., Sayed Ahmed, S.M., Adelsberg, D.C., Carreno,
841 J.M., Strohmeier, S., Schmitz, A.J., Zafar, S., Zhou, J.Q., et al. (2021). SARS-CoV-
842 2 mRNA vaccination induces functionally diverse antibodies to NTD, RBD and S2.
843 *Cell*. 10.1016/j.cell.2021.06.005.
- 844 48. Worobey, M., Han, G.-Z., and Rambaut, A. (2014). Genesis and pathogenesis of
845 the 1918 pandemic H1N1 influenza A virus. *Proc. Natl. Acad. Sci. U. S. A.* *111*,
846 8107–8112. 10.1073/pnas.1324197111.

49. Taubenberger, J.K., and Morens, D.M. (2006). 1918 Influenza: the mother of all pandemics. *Emerg. Infect. Dis.* 12, 15–22. 10.3201/eid1201.050979.
50. Gostic, K.M., Bridge, R., Brady, S., Viboud, C., Worobey, M., and Lloyd-Smith, J.O. (2019). Childhood immune imprinting to influenza A shapes birth year-specific risk during seasonal H1N1 and H3N2 epidemics. *PLoS Pathog.* 15, e1008109. 10.1371/journal.ppat.1008109.
51. Gostic, K.M., Ambrose, M., Worobey, M., and Lloyd-Smith, J.O. (2016). Potent protection against H5N1 and H7N9 influenza via childhood hemagglutinin imprinting. *Science* 354, 722–726. 10.1126/science.aag1322.
52. Greaney, A.J., Eguia, R.T., Starr, T.N., Khan, K., Franko, N., Logue, J.K., Lord, S.M., Speake, C., Chu, H.Y., Sigal, A., et al. (2022). The SARS-CoV-2 Delta variant induces an antibody response largely focused on class 1 and 2 antibody epitopes. *PLoS Pathog.* 18, e1010592. 10.1371/journal.ppat.1010592.
53. Abbott, R.K., Lee, J.H., Menis, S., Skog, P., Rossi, M., Ota, T., Kulp, D.W., Bhullar, D., Kalyuzhniy, O., Havenar-Daughton, C., et al. (2018). Precursor Frequency and Affinity Determine B Cell Competitive Fitness in Germinal Centers, Tested with Germline-Targeting HIV Vaccine Immunogens. *Immunity* 48, 133-146.e6. 10.1016/j.immuni.2017.11.023.
54. Chan, T.D., Gatto, D., Wood, K., Camidge, T., Basten, A., and Brink, R. (2009). Antigen affinity controls rapid T-dependent antibody production by driving the

expansion rather than the differentiation or extrafollicular migration of early
plasmablasts. *J. Immunol.* **183**, 3139–3149. 10.4049/jimmunol.0901690.

55. Anderson, S.M., Khalil, A., Uduman, M., Hershberg, U., Louzoun, Y., Haberman, A.M., Kleinstein, S.H., and Shlomchik, M.J. (2009). Taking advantage: high-affinity B cells in the germinal center have lower death rates, but similar rates of division, compared to low-affinity cells. *J. Immunol.* **183**, 7314–7325. 10.4049/jimmunol.0902452.

56. Shih, T.-A.Y., Meffre, E., Roederer, M., and Nussenzweig, M.C. (2002). Role of BCR affinity in T cell dependent antibody responses in vivo. *Nat. Immunol.* **3**, 570–575. 10.1038/ni803.

57. Yeh, C.-H., Nojima, T., Kuraoka, M., and Kelsoe, G. (2018). Germinal center entry not selection of B cells is controlled by peptide-MHCII complex density. *Nat. Commun.* **9**, 1–11. 10.1038/s41467-018-03382-x.

58. Kwong, P.D., Wyatt, R., Robinson, J., Sweet, R.W., Sodroski, J., and Hendrickson, W.A. (1998). Structure of an HIV gp120 envelope glycoprotein in complex with the CD4 receptor and a neutralizing human antibody. *Nature* **393**, 648–659. 10.1038/31405.

59. Grant, O.C., Montgomery, D., Ito, K., and Woods, R.J. (2020). Analysis of the SARS-CoV-2 spike protein glycan shield reveals implications for immune recognition. *Sci. Rep.* **10**, 14991. 10.1038/s41598-020-71748-7.

60. Chan, T.D., Wood, K., Hermes, J.R., Butt, D., Jolly, C.J., Basten, A., and Brink, R. (2012). Elimination of germinal-center-derived self-reactive B cells is governed by the location and concentration of self-antigen. *Immunity* 37, 893–904. 10.1016/j.immuni.2012.07.017.
61. Reed, J.H., Jackson, J., Christ, D., and Goodnow, C.C. (2016). Clonal redemption of autoantibodies by somatic hypermutation away from self-reactivity during human immunization. *J. Exp. Med.* 213, 1255–1265. 10.1084/jem.20151978.
62. Sabouri, Z., Schofield, P., Horikawa, K., Spierings, E., Kipling, D., Randall, K.L., Langley, D., Roome, B., Vazquez-Lombardi, R., Rouet, R., et al. (2014). Redemption of autoantibodies on anergic B cells by variable-region glycosylation and mutation away from self-reactivity. *Proc. Natl. Acad. Sci. U. S. A.* 111, E2567-75. 10.1073/pnas.1406974111.
63. Sangesland, M., Torrents de la Peña, A., Boyoglu-Barnum, S., Ronsard, L., Mohamed, F.A.N., Moreno, T.B., Barnes, R.M., Rohrer, D., Lonberg, N., Ghebremichael, M., et al. (2022). Allelic polymorphism controls autoreactivity and vaccine elicitation of human broadly neutralizing antibodies against influenza virus. *Immunity* 55, 1693-1709.e8. 10.1016/j.immuni.2022.07.006.
64. Berman, J.E., Nickerson, K.G., Pollock, R.R., Barth, J.E., Schuurman, R.K., Knowles, D.M., Chess, L., and Alt, F.W. (1991). VH gene usage in humans: biased usage of the VH6 gene in immature B lymphoid cells. *Eur. J. Immunol.* 21, 1311–1314. 10.1002/eji.1830210532.

65. Willems van Dijk, K., Milner, L.A., Sasso, E.H., and Milner, E.C. (1992).
Chromosomal organization of the heavy chain variable region gene segments
comprising the human fetal antibody repertoire. *Proc. Natl. Acad. Sci. U. S. A.* **89**,
10430–10434. [10.1073/pnas.89.21.10430](https://doi.org/10.1073/pnas.89.21.10430).
66. Nadel, B., Tang, A., Lugo, G., Love, V., Escuro, G., and Feeney, A.J. (1998).
Decreased frequency of rearrangement due to the synergistic effect of nucleotide
changes in the heptamer and nonamer of the recombination signal sequence of the
V kappa gene A2b, which is associated with increased susceptibility of Navajos to
Haemophilus influenzae type b disease. *J. Immunol.* **161**, 6068–6073.
67. Murray, S.M., Ansari, A.M., Frater, J., Klenerman, P., Dunachie, S., Barnes, E., and
Ogbe, A. (2023). The impact of pre-existing cross-reactive immunity on SARS-CoV-
2 infection and vaccine responses. *Nat. Rev. Immunol.* **23**, 304–316.
[10.1038/s41577-022-00809-x](https://doi.org/10.1038/s41577-022-00809-x).
68. Chemaitelly, H., Ayoub, H.H., Tang, P., Hasan, M.R., Coyle, P., Yassine, H.M., Al-
Khatib, H.A., Smatti, M.K., Al-Kanaani, Z., Al-Kuwari, E., et al. (2022). Immune
Imprinting and Protection against Repeat Reinfection with SARS-CoV-2. *N. Engl. J.*
Med. [10.1056/NEJMc2211055](https://doi.org/10.1056/NEJMc2211055).
69. Koutsakos, M., and Ellebedy, A.H. (2023). Immunological imprinting: Understanding
COVID-19. *Immunity* **56**, 909–913. [10.1016/j.immuni.2023.04.012](https://doi.org/10.1016/j.immuni.2023.04.012).
70. Alsoussi, W.B., Malladi, S.K., Zhou, J.Q., Liu, Z., Ying, B., Kim, W., Schmitz, A.J.,
Lei, T., Horvath, S.C., Sturtz, A.J., et al. (2023). SARS-CoV-2 Omicron boosting

induces de novo B cell response in humans. *Nature* 617, 592–598.

10.1038/s41586-023-06025-4.

71. Cao, Y., Yisimayi, A., Jian, F., Song, W., Xiao, T., Wang, L., Du, S., Wang, J., Li, Q., Chen, X., et al. (2022). BA.2.12.1, BA.4 and BA.5 escape antibodies elicited by Omicron infection. *Nature* 608, 593–602. 10.1038/s41586-022-04980-y.

72. Cao, Y., Jian, F., Wang, J., Yu, Y., Song, W., Yisimayi, A., Wang, J., An, R., Chen, X., Zhang, N., et al. (2023). Imprinted SARS-CoV-2 humoral immunity induces convergent Omicron RBD evolution. *Nature* 614, 521–529. 10.1038/s41586-022-05644-7.

73. Park, Y.-J., Pinto, D., Walls, A.C., Liu, Z., De Marco, A., Benigni, F., Zatta, F., Silacci-Fregni, C., Bassi, J., Sprouse, K.R., et al. (2022). Imprinted antibody responses against SARS-CoV-2 Omicron sublineages. *Science* 378, 619–627. 10.1126/science.adc9127.

74. Reynolds, C.J., Gibbons, J.M., Pade, C., Lin, K.-M., Sandoval, D.M., Pieper, F., Butler, D.K., Liu, S., Otter, A.D., Joy, G., et al. (2022). Heterologous infection and vaccination shapes immunity against SARS-CoV-2 variants. *Science* 375, 183–192. 10.1126/science.abm0811.

75. Gagne, M., Moliva, J.I., Foulds, K.E., Andrew, S.F., Flynn, B.J., Werner, A.P., Wagner, D.A., Teng, I.-T., Lin, B.C., Moore, C., et al. (2022). mRNA-1273 or mRNA-Omicron boost in vaccinated macaques elicits similar B cell expansion,

neutralizing responses, and protection from Omicron. *Cell* **185**, 1556-1571.e18.
10.1016/j.cell.2022.03.038.

76. Masurel, N. (1969). RELATION BETWEEN HONG KONG VIRUS AND FORMER
HUMAN A2 ISOLATES AND THE A/EQUI2 VIRUS IN HUMAN SERA COLLECTED
BEFORE 1957. *Lancet* **293**, 907–910. 10.1016/S0140-6736(69)92544-6.

77. Masurel, N., and Heijntink, R.A. (1983). Recycling of H1N1 influenza A virus in man--
a haemagglutinin antibody study. *J. Hyg.* **90**, 397–402.
10.1017/s0022172400029028.

78. Akinbami, L.J., Kruszon-Moran, D., Wang, C.-Y., Storandt, R.J., Clark, J., Riddles,
M.K., and Mohadjer, L.K. (2022). SARS-CoV-2 serology and self-reported infection
among adults - National Health and Nutrition Examination Survey, United States,
august 2021-may 2022. *MMWR Morb. Mortal. Wkly. Rep.* **71**, 1522–1525.
10.15585/mmwr.mm7148a4.

79. Zhang, Z., Mateus, J., Coelho, C.H., Dan, J.M., Moderbacher, C.R., Gálvez, R.I.,
Cortes, F.H., Grifoni, A., Tarke, A., Chang, J., et al. (2022). Humoral and cellular
immune memory to four COVID-19 vaccines. *Cell* **185**, 2434-2451.e17.
10.1016/j.cell.2022.05.022.

80. Jones, J.M., Manrique, I.M., Stone, M.S., Grebe, E., Saa, P., Germanio, C.D.,
Spencer, B.R., Notari, E., Bravo, M., Lanteri, M.C., et al. (2023). Estimates of
SARS-CoV-2 seroprevalence and incidence of primary SARS-CoV-2 infections
among blood donors, by COVID-19 vaccination status - United States, April 2021-

September 2022. *MMWR Morb. Mortal. Wkly. Rep.* 72, 601–605.

10.15585/mmwr.mm7222a3.

81. Kaplonek, P., Fischinger, S., Cizmeci, D., Bartsch, Y.C., Kang, J., Burke, J.S., Shin, S.A., Dayal, D., Martin, P., Mann, C., et al. (2022). mRNA-1273 vaccine-induced antibodies maintain Fc-effector functions across SARS-CoV-2 Variants of Concern. *Immunity*. 10.1016/j.immuni.2022.01.001.

82. Lutrick, K., Ellingson, K.D., Baccam, Z., Rivers, P., Beitel, S., Parker, J., Hollister, J., Sun, X., Gerald, J.K., Komatsu, K., et al. (2021). COVID-19 infection, reinfection, and vaccine effectiveness in a prospective cohort of Arizona frontline/essential workers: The AZ HEROES research protocol. *JMIR Res. Protoc.* 10, e28925. 10.2196/28925.

83. Goel, R.R., Apostolidis, S.A., Painter, M.M., Mathew, D., Pattekar, A., Kuthuru, O., Gouma, S., Hicks, P., Meng, W., Rosenfeld, A.M., et al. (2021). Distinct antibody and memory B cell responses in SARS-CoV-2 naïve and recovered individuals following mRNA vaccination. *Sci Immunol* 6. 10.1126/sciimmunol.abi6950.

84. Edwards, L.J., Fowlkes, A.L., Wesley, M.G., Kuntz, J.L., Odean, M.J., Caban-Martinez, A.J., Dunnigan, K., Phillips, A.L., Grant, L., Herring, M.K., et al. (2021). “Research on the Epidemiology of SARS-CoV-2 in Essential Response Personnel (RECOVER) Study: Protocol for a multi-site longitudinal cohort.” *JMIR Res Protoc* 7.

- 990 85. Greaney, A.J., Loes, A.N., Gentles, L.E., Crawford, K.H.D., Starr, T.N., Malone,
991 K.D., Chu, H.Y., and Bloom, J.D. (2021). Antibodies elicited by mRNA-1273
992 vaccination bind more broadly to the receptor binding domain than do those from
993 SARS-CoV-2 infection. *Science Translational Medicine*.
994 10.1126/scitranslmed.abi9915.
- 995 86. Rambaut, A., Holmes, E.C., O'Toole, Á., Hill, V., McCrone, J.T., Ruis, C., du
996 Plessis, L., and Pybus, O.G. (2020). A dynamic nomenclature proposal for SARS-
997 CoV-2 lineages to assist genomic epidemiology. *Nat. Microbiol.* 5, 1403–1407.
998 10.1038/s41564-020-0770-5.
- 999 87. Cherian, S., Potdar, V., Jadhav, S., Yadav, P., Gupta, N., Das, M., Rakshit, P.,
1000 Singh, S., Abraham, P., Panda, S., et al. (2021). SARS-CoV-2 spike mutations,
1001 L452R, T478K, E484Q and P681R, in the second wave of COVID-19 in
1002 Maharashtra, India. *Microorganisms* 9, 1542. 10.3390/microorganisms9071542.
- 1003 88. Ripperger, T.J., Uhrlaub, J.L., Watanabe, M., Wong, R., Castaneda, Y., Pizzato,
1004 H.A., Thompson, M.R., Bradshaw, C., Weinkauf, C.C., Bime, C., et al. (2020).
1005 Orthogonal SARS-CoV-2 Serological Assays Enable Surveillance of Low-
1006 Prevalence Communities and Reveal Durable Humoral Immunity. *Immunity* 53,
1007 925-933.e4. 10.1016/j.immuni.2020.10.004.
- 1008 89. Piccoli, L., Park, Y.-J., Tortorici, M.A., Czudnochowski, N., Walls, A.C., Beltramello,
1009 M., Silacci-Fregni, C., Pinto, D., Rosen, L.E., Bowen, J.E., et al. (2020). Mapping
1010 Neutralizing and Immunodominant Sites on the SARS-CoV-2 Spike Receptor-

- 1011 Binding Domain by Structure-Guided High-Resolution Serology. *Cell* **183**, 1024-
1012 1042.e21. 10.1016/j.cell.2020.09.037.
- 1013 90. Greaney, A.J., Loes, A.N., Crawford, K.H.D., Starr, T.N., Malone, K.D., Chu, H.Y.,
1014 and Bloom, J.D. (2021). Comprehensive mapping of mutations in the SARS-CoV-2
1015 receptor-binding domain that affect recognition by polyclonal human plasma
1016 antibodies. *Cell Host Microbe* **29**, 463-476.e6. 10.1016/j.chom.2021.02.003.
- 1017 91. Röltgen, K., Nielsen, S.C.A., Silva, O., Younes, S.F., Zaslavsky, M., Costales, C.,
1018 Yang, F., Wirz, O.F., Solis, D., Hoh, R.A., et al. (2022). Immune imprinting, breadth
1019 of variant recognition, and germinal center response in human SARS-CoV-2
1020 infection and vaccination. *Cell* **185**, 1025-1040.e14. 10.1016/j.cell.2022.01.018.
- 1021 92. Suryadevara, N., Shrihari, S., Gilchuk, P., VanBlargan, L.A., Binshtein, E., Zost,
1022 S.J., Nargi, R.S., Sutton, R.E., Winkler, E.S., Chen, E.C., et al. (2021). Neutralizing
1023 and protective human monoclonal antibodies recognizing the N-terminal domain of
1024 the SARS-CoV-2 spike protein. *Cell* **184**, 2316-2331.e15.
1025 10.1016/j.cell.2021.03.029.
- 1026 93. Cerutti, G., Guo, Y., Zhou, T., Gorman, J., Lee, M., Rapp, M., Reddem, E.R., Yu, J.,
1027 Bahna, F., Bimela, J., et al. (2021). Potent SARS-CoV-2 neutralizing antibodies
1028 directed against spike N-terminal domain target a single supersite. *Cell Host*
1029 *Microbe* **29**, 819-833.e7. 10.1016/j.chom.2021.03.005.
- 1030 94. McCallum, M., De Marco, A., Lempp, F.A., Tortorici, M.A., Pinto, D., Walls, A.C.,
1031 Beltramello, M., Chen, A., Liu, Z., Zatta, F., et al. (2021). N-terminal domain

1032 antigenic mapping reveals a site of vulnerability for SARS-CoV-2. *Cell* **184**, 2332-
1033 2347.e16. 10.1016/j.cell.2021.03.028.

1034 95. Shroff, R.T., Chalasani, P., Wei, R., Pennington, D., Quirk, G., Schoenle, M.V.,
1035 Peyton, K.L., Uhrlaub, J.L., Ripperger, T.J., Jergović, M., et al. (2021). Immune
1036 responses to two and three doses of the BNT162b2 mRNA vaccine in adults with
1037 solid tumors. *Nat. Med.*, 1–10. 10.1038/s41591-021-01542-z.

1038 96. Motozono, C., Toyoda, M., Zahradnik, J., Saito, A., Nasser, H., Tan, T.S., Ngare, I.,
1039 Kimura, I., Uriu, K., Kosugi, Y., et al. (2021). SARS-CoV-2 spike L452R variant
1040 evades cellular immunity and increases infectivity. *Cell Host Microbe*.
1041 10.1016/j.chom.2021.06.006.

1042 97. He, P., Liu, B., Gao, X., Yan, Q., Pei, R., Sun, J., Chen, Q., Hou, R., Li, Z., Zhang,
1043 Y., et al. (2022). SARS-CoV-2 Delta and Omicron variants evade population
1044 antibody response by mutations in a single spike epitope. *Nat Microbiol*.
1045 10.1038/s41564-022-01235-4.

1046 98. Tchesnokova, V., Kulasekara, H., Larson, L., Bowers, V., Rechkina, E., Kisiela, D.,
1047 Sledneva, Y., Choudhury, D., Maslova, I., Deng, K., et al. (2021). Acquisition of the
1048 L452R mutation in the ACE2-binding interface of spike protein triggers recent
1049 massive expansion of SARS-CoV-2 variants. *J. Clin. Microbiol.* **59**, e0092121.
1050 10.1128/JCM.00921-21.

1051 99. Greaney, A.J., Starr, T.N., Eguia, R.T., Loes, A.N., Khan, K., Karim, F., Cele, S.,
1052 Bowen, J.E., Logue, J.K., Corti, D., et al. (2022). A SARS-CoV-2 variant elicits an

1053 antibody response with a shifted immunodominance hierarchy. *PLoS Pathog.* **18**,
1054 e1010248. 10.1371/journal.ppat.1010248.

1055 100. Setliff, I., Shiakolas, A.R., Pilewski, K.A., Murji, A.A., Mapengo, R.E., Janowska,
1056 K., Richardson, S., Oosthuysen, C., Raju, N., Ronsard, L., et al. (2019). High-
1057 Throughput Mapping of B Cell Receptor Sequences to Antigen Specificity. *Cell* **179**,
1058 1636-1646.e15. 10.1016/j.cell.2019.11.003.

1059 101. Schiepers, A., van 't Wout, M.F.L., Greaney, A.J., Zang, T., Muramatsu, H., Lin,
1060 P.J.C., Tam, Y.K., Mesin, L., Starr, T.N., Bieniasz, P.D., et al. (2023). Molecular
1061 fate-mapping of serum antibody responses to repeat immunization. *Nature*.
1062 10.1038/s41586-023-05715-3.

1063 102. Horwitz, L.I., Thaweethai, T., Brosnahan, S.B., Cicek, M.S., Fitzgerald, M.L.,
1064 Goldman, J.D., Hess, R., Hodder, S.L., Jacoby, V.L., Jordan, M.R., et al. (2023).
1065 Researching COVID to Enhance Recovery (RECOVER) adult study protocol:
1066 Rationale, objectives, and design. *PLoS One* **18**, e0286297.
1067 10.1371/journal.pone.0286297.

1068 103. Smith, K.G., Light, A., Nossal, G.J., and Tarlinton, D.M. (1997). The extent of
1069 affinity maturation differs between the memory and antibody-forming cell
1070 compartments in the primary immune response. *EMBO J.* **16**, 2996–3006.
1071 10.1093/emboj/16.11.2996.

1072 104. Lavinder, J.J., Wine, Y., Giesecke, C., Ippolito, G.C., Horton, A.P., Lungu, O.I.,
1073 Hoi, K.H., DeKosky, B.J., Murrin, E.M., Wirth, M.M., et al. (2014). Identification and

1074 characterization of the constituent human serum antibodies elicited by vaccination.
1075 Proc. Natl. Acad. Sci. U. S. A. *111*, 2259–2264. 10.1073/pnas.1317793111.

1076 105. Pape, K.A., Maul, R.W., Dileepan, T., Paustian, A.S., Gearhart, P.J., and
1077 Jenkins, M.K. (2018). Naive B cells with high-avidity germline-encoded antigen
1078 receptors produce persistent IgM+ and transient IgG+ memory B cells. *Immunity* *48*,
1079 1135-1143.e4. 10.1016/j.immuni.2018.04.019.

1080 106. Andrews, S.F., Kaur, K., Pauli, N.T., Huang, M., Huang, Y., and Wilson, P.C.
1081 (2015). High preexisting serological antibody levels correlate with diversification of
1082 the influenza vaccine response. *J. Virol.* *89*, 3308–3317. 10.1128/JVI.02871-14.

1083 107. Inoue, T., Shinnakasu, R., Kawai, C., Yamamoto, H., Sakakibara, S., Ono, C.,
1084 Itoh, Y., Terooatea, T., Yamashita, K., Okamoto, T., et al. (2023). Antibody
1085 feedback contributes to facilitating the development of Omicron-reactive memory B
1086 cells in SARS-CoV-2 mRNA vaccinees. *J. Exp. Med.* *220*. 10.1084/jem.20221786.

1087 108. Liu, Y.J., Zhang, J., Lane, P.J., Chan, E.Y., and MacLennan, I.C. (1991). Sites of
1088 specific B cell activation in primary and secondary responses to T cell-dependent
1089 and T cell-independent antigens. *Eur. J. Immunol.* *21*, 2951–2962.
1090 10.1002/eji.1830211209.

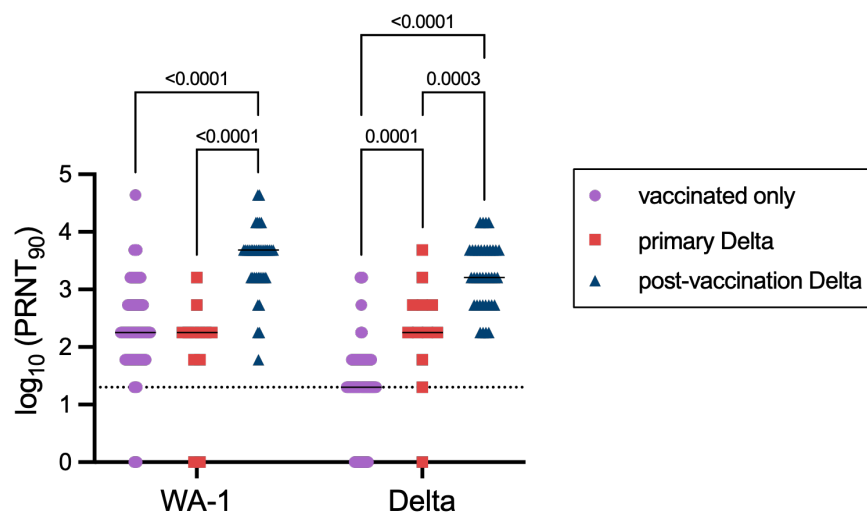
1091 109. Abbott, R.K., and Crotty, S. (2020). Factors in B cell competition and
1092 immunodominance. *Immunol. Rev.* *296*, 120–131. 10.1111/imr.12861.

1093 110. Krammer, F. (2019). The human antibody response to influenza A virus infection
1094 and vaccination. *Nat. Rev. Immunol.* *19*, 383–397. 10.1038/s41577-019-0143-6.

- 1095 111. Chia, P.Y., Ong, S.W.X., Chiew, C.J., Ang, L.W., Chavatte, J.-M., Mak, T.-M.,
1096 Cui, L., Kalimuddin, S., Chia, W.N., Tan, C.W., et al. (2022). Virological and
1097 serological kinetics of SARS-CoV-2 Delta variant vaccine breakthrough infections: a
1098 multicentre cohort study. *Clin. Microbiol. Infect.* 28, 612.e1-612.e7.
1099 10.1016/j.cmi.2021.11.010.
- 1100 112. Schaefer-Babajew, D., Wang, Z., Muecksch, F., Cho, A., Loewe, M., Cipolla, M.,
1101 Raspe, R., Johnson, B., Canis, M., DaSilva, J., et al. (2023). Antibody feedback
1102 regulates immune memory after SARS-CoV-2 mRNA vaccination. *Nature* 613, 735–
1103 742. 10.1038/s41586-022-05609-w.
- 1104 113. Gao, Y., Cai, C., Grifoni, A., Müller, T.R., Niessl, J., Olofsson, A., Humbert, M.,
1105 Hansson, L., Österborg, A., Bergman, P., et al. (2022). Ancestral SARS-CoV-2-
1106 specific T cells cross-recognize the Omicron variant. *Nat. Med.* 28, 472–476.
1107 10.1038/s41591-022-01700-x.
- 1108 114. Keeton, R., Tincho, M.B., Ngomti, A., Baguma, R., Benede, N., Suzuki, A., Khan,
1109 K., Cele, S., Bernstein, M., Karim, F., et al. (2022). T cell responses to SARS-CoV-2
1110 spike cross-recognize Omicron. *Nature* 603, 488–492. 10.1038/s41586-022-04460-
1111 3.
- 1112 115. Bartsch, Y.C., Wang, C., Zohar, T., Fischinger, S., Atyeo, C., Burke, J.S., Kang,
1113 J., Edlow, A.G., Fasano, A., Baden, L.R., et al. (2021). Humoral signatures of
1114 protective and pathological SARS-CoV-2 infection in children. *Nat. Med.* 27, 454–
1115 462. 10.1038/s41591-021-01263-3.

- 1116 116. Ying, B., Scheaffer, S.M., Whitener, B., Liang, C.-Y., Dmytrenko, O., Mackin, S.,
1117 Wu, K., Lee, D., Avena, L.E., Chong, Z., et al. (2022). Boosting with Omicron-
1118 matched or historical mRNA vaccines increases neutralizing antibody responses
1119 and protection against B.1.1.529 infection in mice. *bioRxiv*org, 2022.02.07.479419.
1120 10.1101/2022.02.07.479419.
- 1121 117. Barnes, C.O., West, A.P., Jr, Huey-Tubman, K.E., Hoffmann, M.A.G., Sharaf,
1122 N.G., Hoffman, P.R., Koranda, N., Gristick, H.B., Gaebler, C., Muecksch, F., et al.
1123 (2020). Structures of Human Antibodies Bound to SARS-CoV-2 Spike Reveal
1124 Common Epitopes and Recurrent Features of Antibodies. *Cell* 182, 828-842.e16.
1125 10.1016/j.cell.2020.06.025.
- 1126 118. Hay, J.A., Kissler, S.M., Fauver, J.R., Mack, C., Tai, C.G., Samant, R.M.,
1127 Connolly, S., Anderson, D.J., Khullar, G., MacKay, M., et al. (2022). Quantifying the
1128 impact of immune history and variant on SARS-CoV-2 viral kinetics and infection
1129 rebound: A retrospective cohort study. *Elife* 11. 10.7554/eLife.81849.
- 1130 119. Goldfarb, D.M., Tilley, P., Al-Rawahi, G.N., Srigley, J.A., Ford, G., Pedersen, H.,
1131 Pabbi, A., Hannam-Clark, S., Charles, M., Dittrick, M., et al. (2020). Self-collected
1132 saline gargle samples as an alternative to healthcare worker collected
1133 nasopharyngeal swabs for COVID-19 diagnosis in outpatients. *J. Clin. Microbiol.*,
1134 2020.09.13.20188334. 10.1101/2020.09.13.20188334.
- 1135 120. Hao, Y., Hao, S., Andersen-Nissen, E., Mauck, W.M., 3rd, Zheng, S., Butler, A.,
1136 Lee, M.J., Wilk, A.J., Darby, C., Zager, M., et al. (2021). Integrated analysis of
1137 multimodal single-cell data. *Cell* 184, 3573-3587.e29. 10.1016/j.cell.2021.04.048.

A.



B.

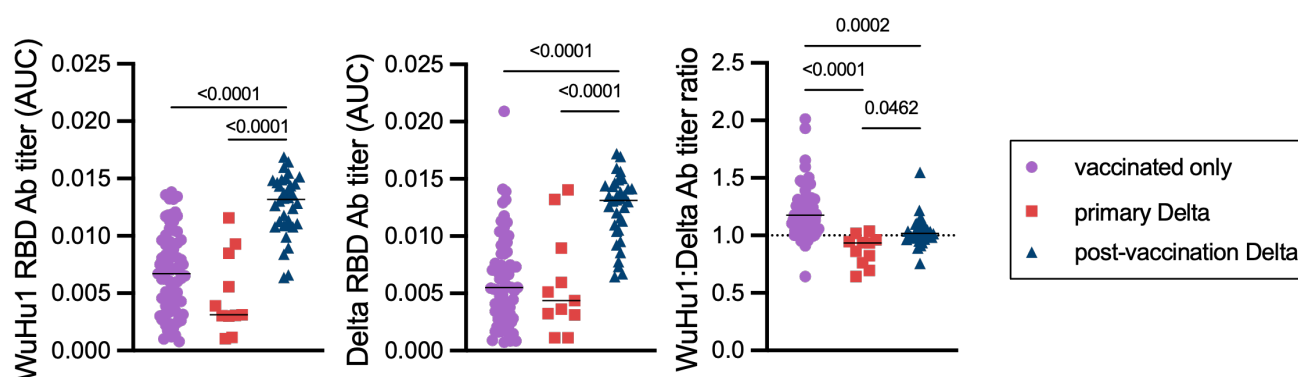
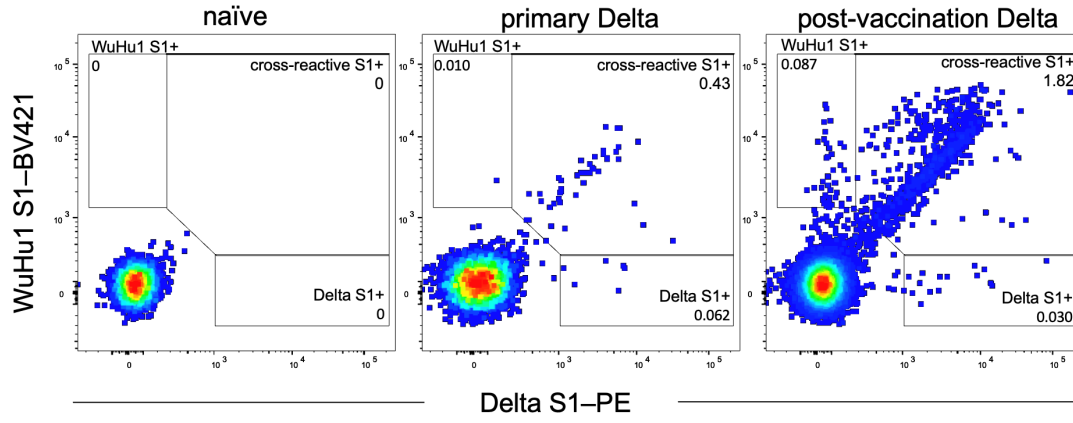
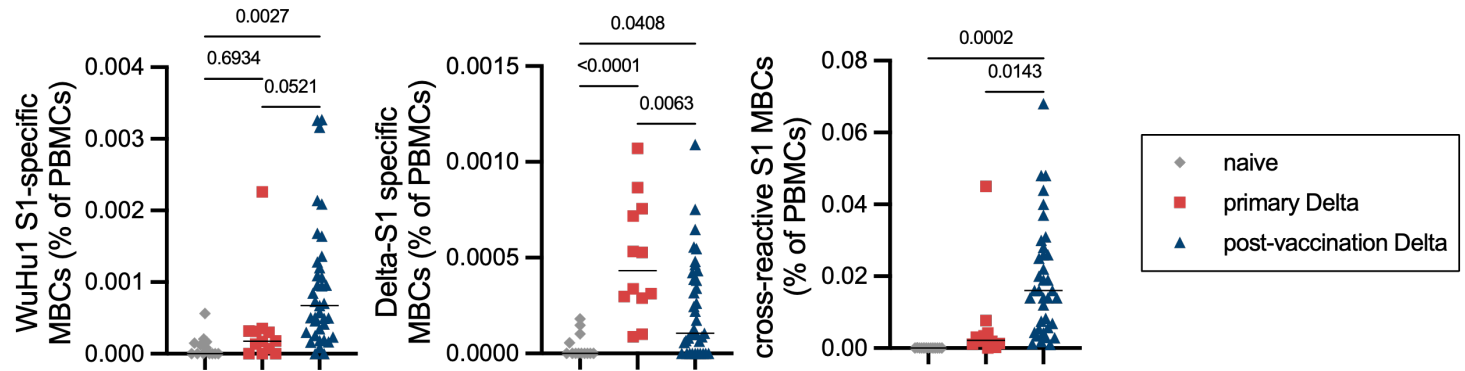


Figure 1. Primary and recall antibody responses to Wuhan and Delta strains of SARS-COV-2. (A) Virus neutralization assays were performed using the WA-1 and Delta isolates of SARS-CoV-2. Serial 1:3 dilutions of serums were performed and tested for the ability to prevent plaque formation on Vero cells. The lowest concentration capable of preventing more than 90% of plaques was considered to be the PRNT₉₀ value. Each symbol represents an individual. Two-sided P values from t-test statistics were calculated for pairwise differences using two-way ANOVA. Post hoc testing for multiple comparisons between draws was performed using Tukey's multiple comparisons test. P values greater than 0.05 are not depicted. **(B)** Quantitative titers of WuHu1- and Delta RBD-specific antibodies. Serum was initially diluted 1:60, serially diluted 1:3, assessed by ELISA for binding to the listed antigens, and area under the curve (AUC) values were calculated. Each symbol represents an individual. WuHu1 AUC values were divided by their Delta AUC titer in the same individual to calculate a WuHu1:Delta RBD ratio in the rightmost panel. Two-sided P values from t-test statistics were calculated for pairwise differences using one-way ANOVA. Post hoc testing for multiple comparisons between draws was performed using Tukey's multiple comparisons test. P values greater than 0.05 are not depicted.

A.



B.



C.

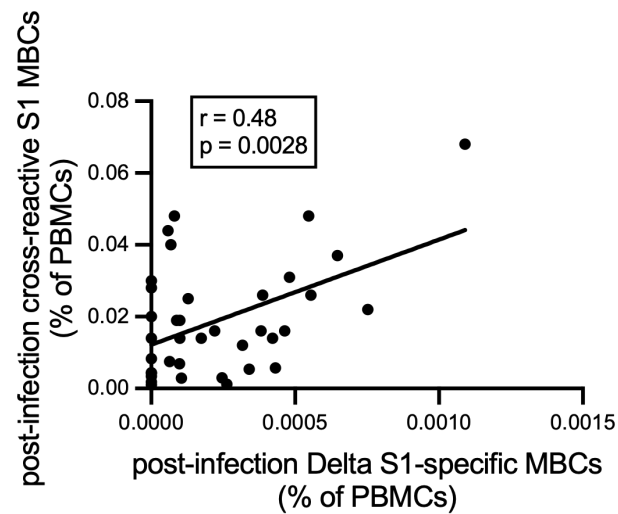
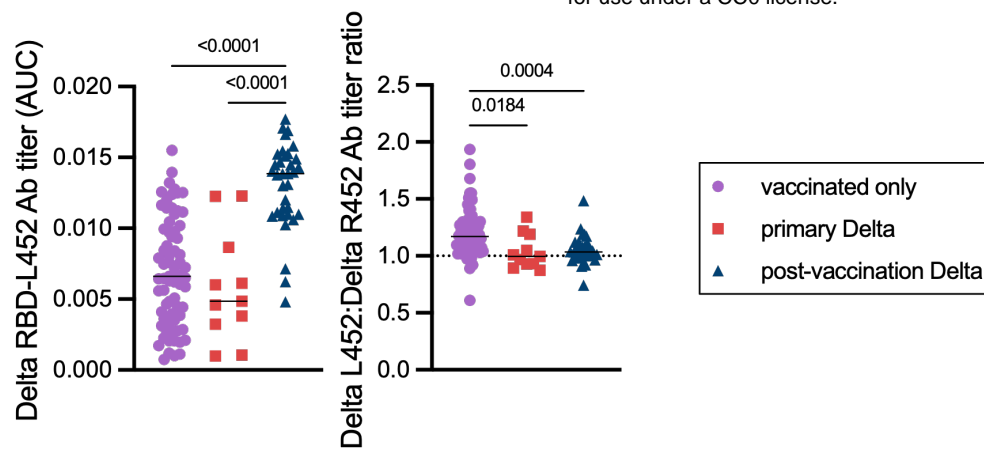
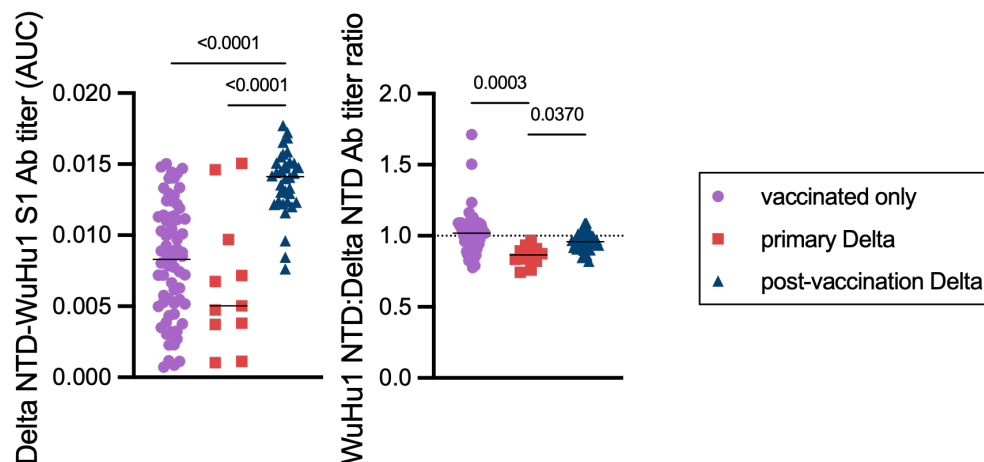


Figure 2. WuHu1 and Delta Memory B cell flow cytometric analysis and quantification. (A) Representative flow cytometric plots of Wuhu1 and Delta S1-specific memory B cells (full gating strategy shown in Figure S2) in naïve, primary Delta infection, and post-vaccination Delta infection cohorts. Cells that bind both WuHu1 S1 and Delta S1 are annotated as cross-reactive S1+, whereas cells that bind only WuHu1 S1 or Delta S1 are annotated as WuHu1 S1+ or Delta S1+, respectively. **(B)** Quantification of isotype-switched memory B cells as a percentage of total PBMCs for WuHu1 S1+, Delta S1+ and cross-reactive S1+ specificities for each cohort of SARS-CoV-2 immune histories. Each symbol represents an individual. Two-sided P values from t-test statistics were calculated for pairwise differences using one-way ANOVA. Post hoc testing for multiple comparisons between draws was performed using Tukey's multiple comparisons test. P values greater than 0.05 are not depicted. **(C)** Correlation of post-infection cross-reactive S1 MBCs (calculated as in Figure 2B) plotted against the frequency of post-infection Delta S1-specific MBCs (calculated as in Figure 2B) in individuals that experienced a post-vaccination Delta infection. Pearson correlation analysis was performed.

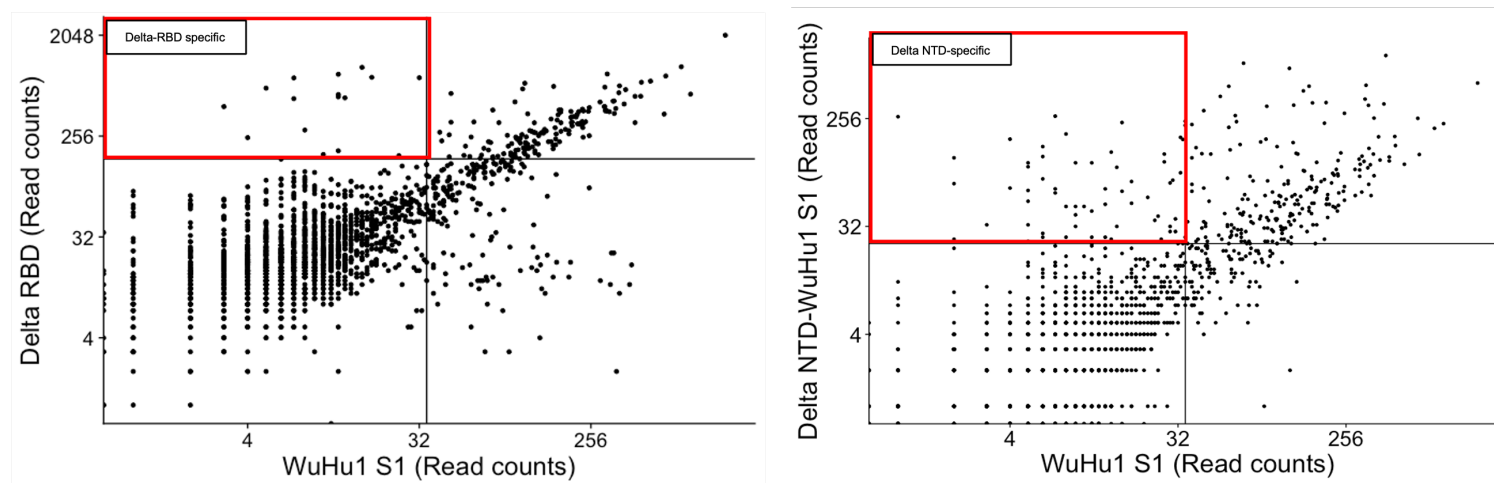
A.



B.



C.



D.

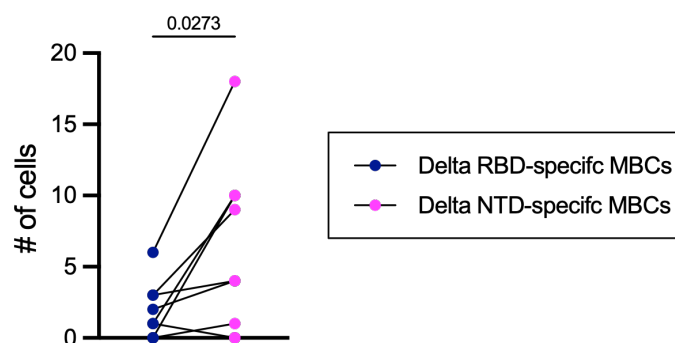
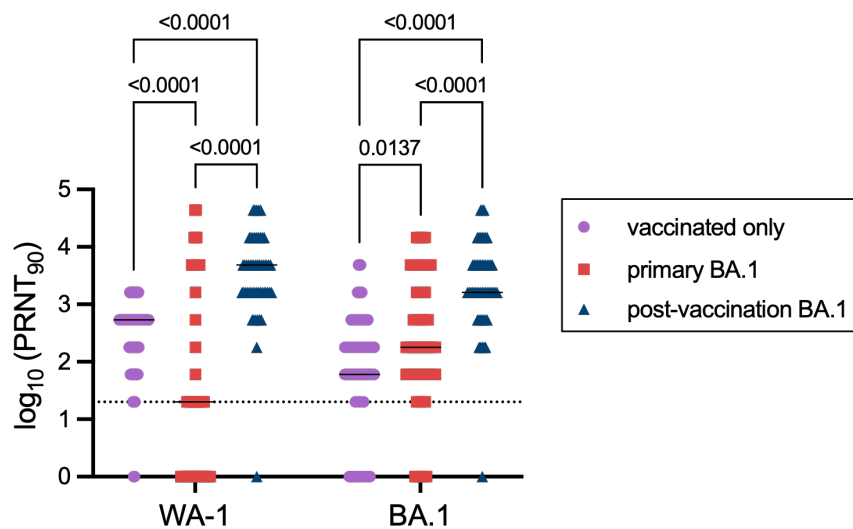


Figure 3. Epitope-specific quantification of Delta RBD- and Delta NTD-specific antibodies and memory B cells. (A) A chimeric protein (Delta RBD-L452) was generated in which R452 was reverted to the ancestral L452. ELISAs were used to quantify serum antibodies that bound to Delta RBD-L452 in each cohort. Delta RBD-L452 AUC titers were divided by Delta RBD titers (Figure 1B) in the same individuals to calculate a L452:R452 titer ratio. Each symbol represents an individual. Two-sided P values from t-test statistics were calculated for pairwise differences using one-way ANOVA. Post hoc testing for multiple comparisons between draws was performed using Tukey's multiple comparisons test. P values greater than 0.05 are not depicted. **(B)** A chimeric protein (Delta NTD-WuHu1 S1) was generated in which Delta NTD mutated epitopes (T19R, G142D, E156-, F157-, R158G) were incorporated into the otherwise WuHu1 S1 backbone. ELISAs were used to quantify serum antibodies that bound to Delta NTD-WuHu1 S1 in each cohort. Delta RBD-L452 AUC titers were divided by their Delta RBD (Supplemental Fig 1A) titer to calculate a WuHu1 NTD:Delta NTD titer ratio. Each symbol represents an individual. Two-sided P values from t-test statistics were calculated for pairwise differences using one-way ANOVA. Post hoc testing for multiple comparisons between draws was performed using Tukey's multiple comparisons test. P values greater than 0.05 are not depicted. **(C)** LIBRA-seq plots of isotype-switched memory B cells enriched for Spike-binding specificities from primary Delta infections. Read count thresholds to determine positivity were set using samples in which cells lacking Spike-binding specificities were sorted and sequenced. Plots are concatenated from ten individuals. **(D)** Quantification of Delta RBD-specific and Delta NTD-specific memory B cells (MBCs) in individuals that experienced a primary Delta infection. Lines

1198 connect specificities within the same individual. Delta RBD-specific cells were classified
1199 by cells that had Delta RBD read counts of greater than 160 and WuHu1 S1 read
1200 counts of less than 35. Delta NTD-specific cells were classified by cells that had Delta
1201 NTD-WuHu1 S1 read counts of greater than 23 and WuHu1 S1 read counts of less than
1202 35. Two-sided P values were calculated for pairwise differences using paired t-tests.
1203
1204
1205
1206
1207

Figure 4

A.



B.

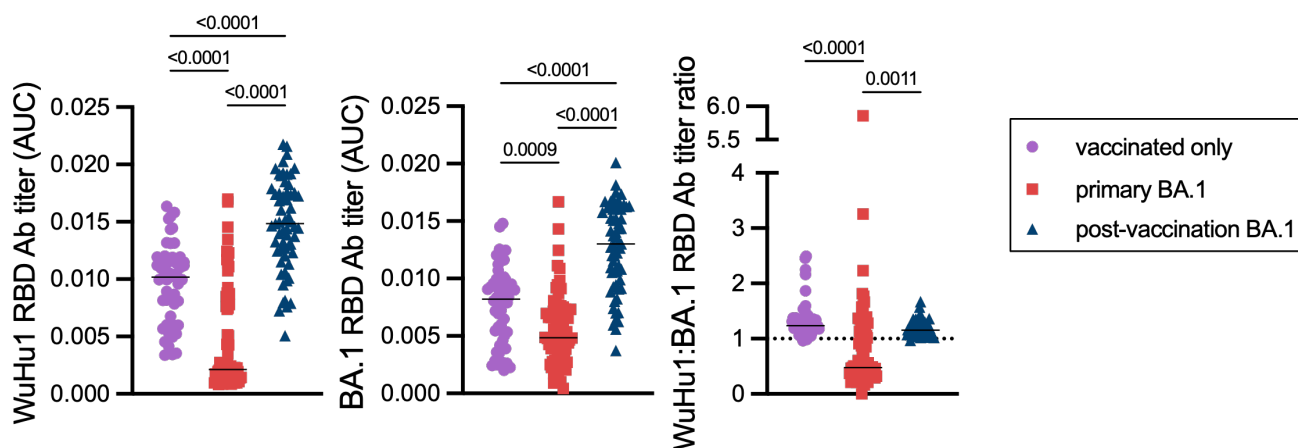


Figure 4. Primary and recall antibody responses to Wuhan and BA.1 strains of

SARS-COV-2. (A) Virus neutralization assays were performed using the WA-1 and

BA.1 isolates of SARS-CoV-2. Serial 1:3 dilutions of serums were performed and tested

for the ability to prevent plaque formation on Vero cells. The lowest concentration

capable of preventing more than 90% of plaques was considered to the PRNT₉₀ value.

Each symbol represents an individual. Two-sided P values from t-test statistics were

calculated for pairwise differences using two-way ANOVA. Post hoc testing for multiple

comparisons between draws was performed using Tukey's multiple comparisons test. P

values greater than 0.05 are not depicted. **(B)** Quantitative titers of Wuhu1 and BA.1

RBD antibodies. Serum was initially diluted 1:60, serially diluted 1:3, assessed by

ELISA for binding to the listed antigens, and area under the curve (AUC) values were

calculated. Each symbol represents an individual. WuHu1 AUC values were divided by

their BA.1 RBD AUC titer in the same individual to calculate a ratio in the rightmost

panel. Two-sided P values from t-test statistics were calculated for pairwise differences

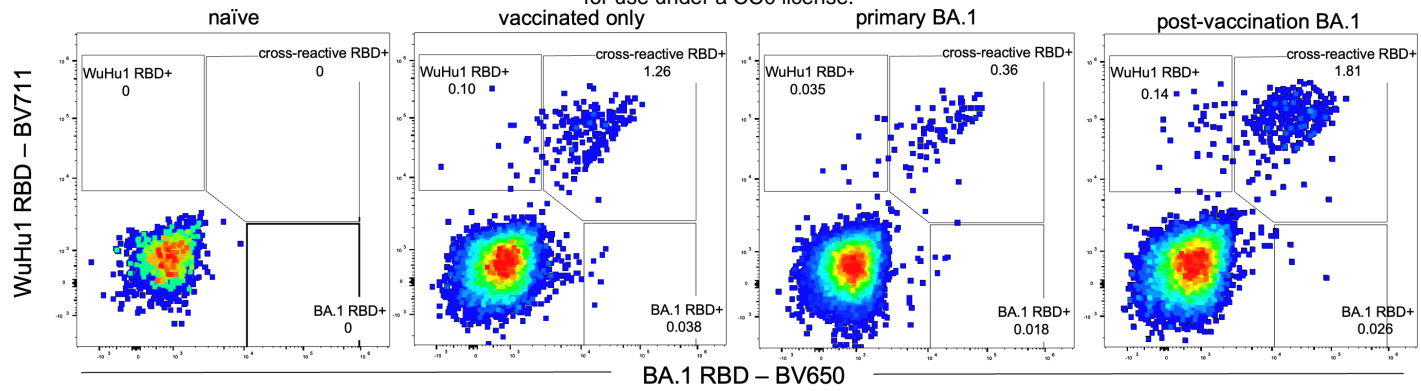
using one-way ANOVA. Post hoc testing for multiple comparisons between draws was

performed using Tukey's multiple comparisons test. P values greater than 0.05 are not

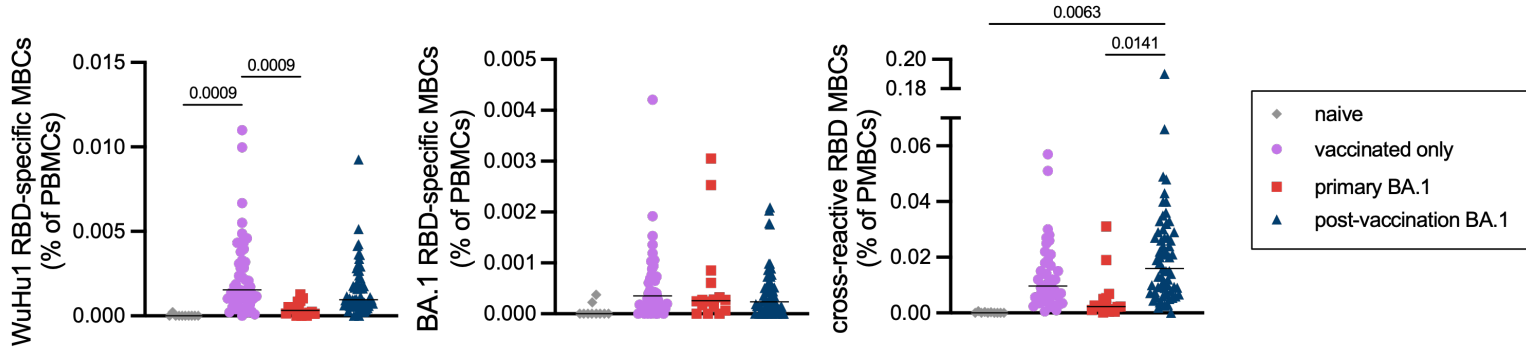
depicted.

Figure 5

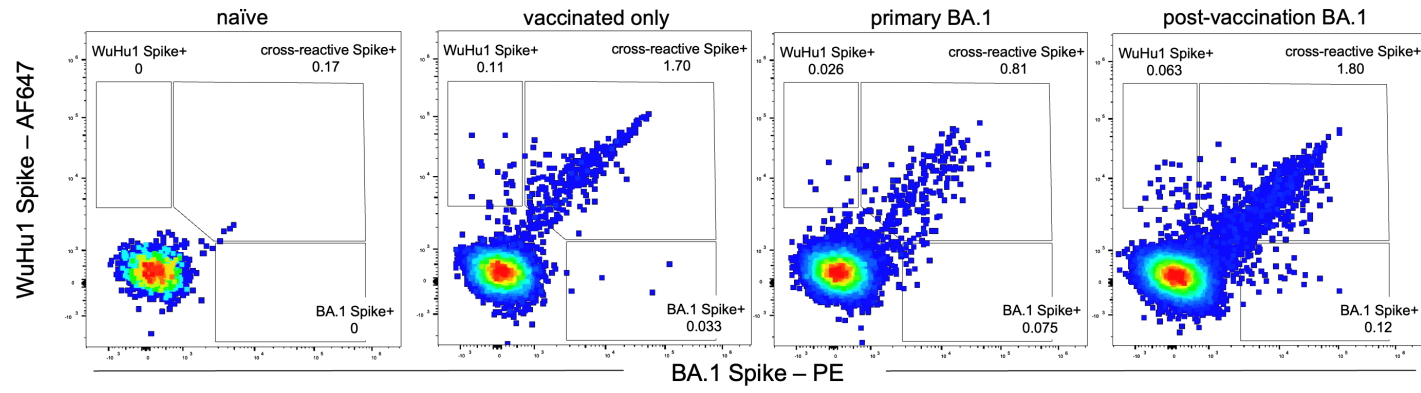
A.



B.



C.



D.

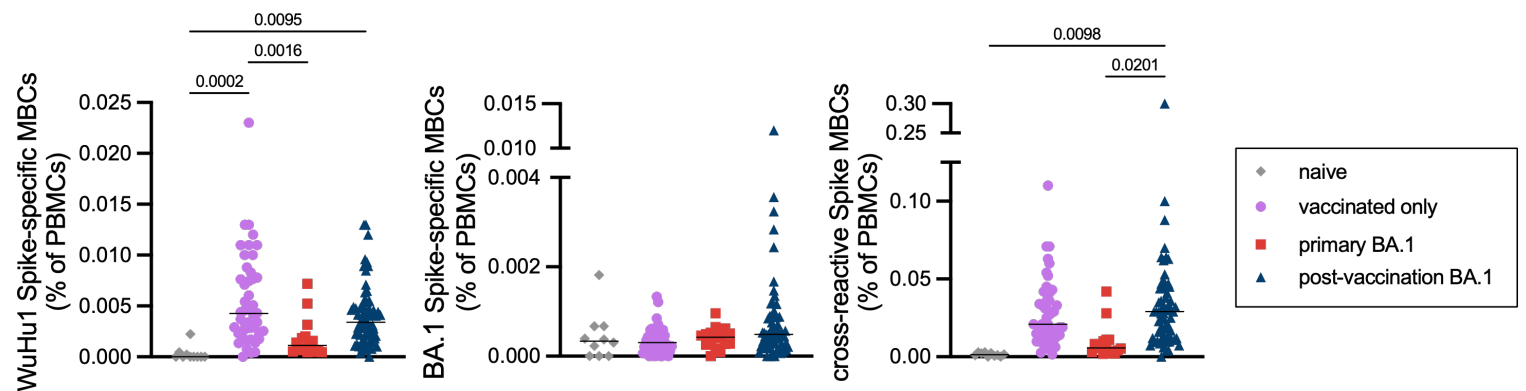
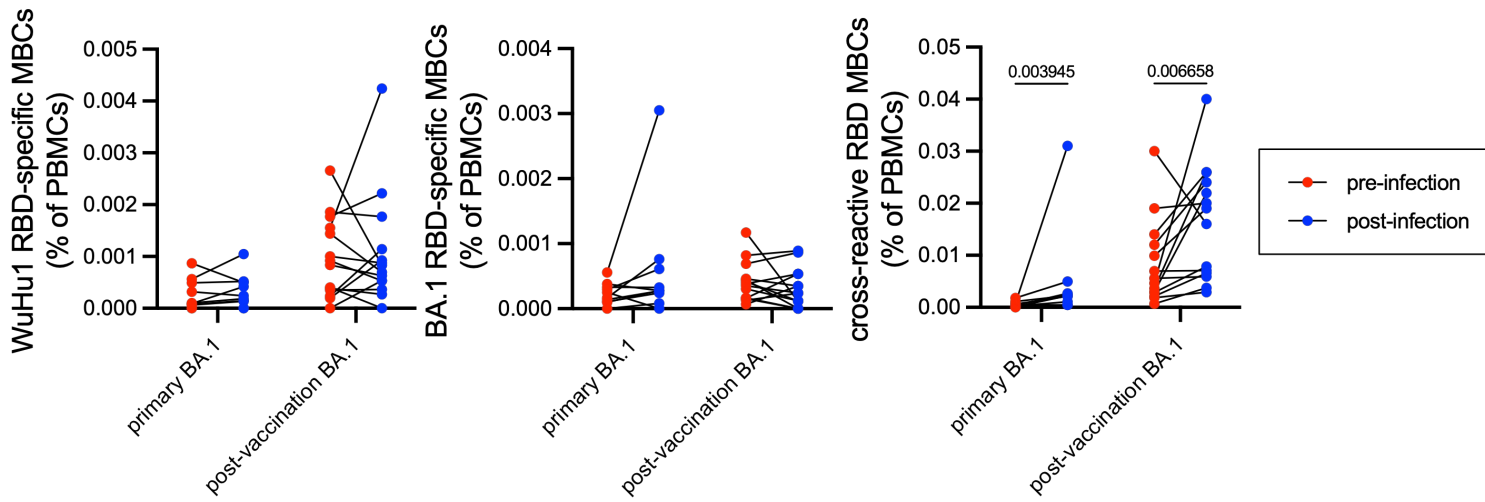


Figure 5. WuHu1 and BA.1 Memory B cell flow cytometric analysis and

quantification. (A) Representative flow cytometric plots of Wuhu1 and BA.1 RBD-specific memory B cells (full gating strategy shown in Figure S3) in naïve, vaccinated only, primary BA.1 infection, and post-vaccination BA.1 infection cohorts. Cells that bind both WuHu1 RBD and BA.1 RBD are annotated as cross-reactive RBD+, whereas cells that bind only WuHu1 RBD or BA.1 RBD are annotated as WuHu1 RBD+ or BA.1 RBD+, respectively. **(B)** Quantification of isotype-switched memory B cells for WuHu1 RBD+, BA.1 RBD+ and cross-reactive RBD+ specificities for each cohort of SARS-CoV-2 immune histories. Each symbol represents an individual. Two-sided P values from t-test statistics were calculated for pairwise differences using one-way ANOVA. Post hoc testing for multiple comparisons between draws was performed using Tukey's multiple comparisons test. P values greater than 0.05 are not depicted. **(C)** Representative flow cytometric plots of Wuhu1 and BA.1 Spike-specific memory B cells (full gating strategy shown in Figure S3) in naïve, vaccinated only, primary BA.1 infection, and post-vaccination BA.1 infection cohorts. Cells that bind both WuHu1 RBD and BA.1 Spike are annotated as cross-reactive Spike+, whereas cells that bind only WuHu1 Spike or BA.1 Spike are annotated as WuHu1 Spike+ or BA.1 Spike+, respectively. **(D)** Quantification of isotype-switched memory B cells for WuHu1 Spike+, BA.1 Spike+ and cross-reactive Spike+ specificities for each cohort of SARS-CoV-2 immune histories. Each symbol represents an individual. Two-sided P values from t-test statistics were calculated for pairwise differences using one-way ANOVA. Post hoc testing for multiple comparisons between draws was performed using Tukey's multiple comparisons test. P values greater than 0.05 are not depicted.

Figure 6

A.



B.

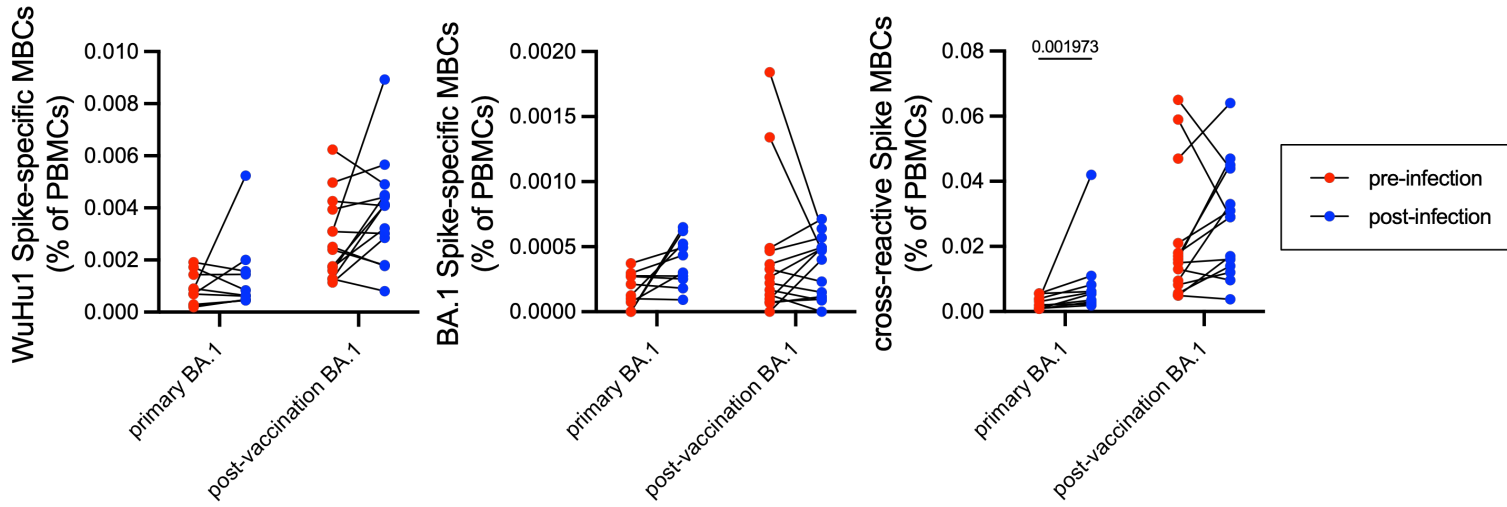


Figure 6. Frequency of WuHu1- and BA.1-specific memory B cells before and after

BA.1 infection. (A) Frequencies of isotype-switched memory B cells with Wuhu1

RBD+, BA.1 RBD+ and cross-reactive RBD+ specificities in both unvaccinated and

vaccinated individuals before and after BA.1 infection. Lines connect the same

individual from pre-infection frequency to post-infection frequency. In primary infections,

pre-infection blood draws were taken on average 75.6 days before infection and post-

infection blood draws occurred on 37.8 days after infection. In post-vaccination

infections, pre-infection blood draws were taken on average 87.6 days before infection

and post-infection draws were taken an average of 38.3 days after infection. Individuals

that received a vaccine after the pre-infection draw were excluded from analysis. P

values were calculated using Wilcoxon matched-pairs signed rank test on each row and

post hoc testing for multiple comparisons between draws was performed using two-

stage linear step-up procedure of Benjamini, Krieger and Yekutieli. P values greater

than 0.05 are not depicted. **(B)** Frequencies of isotype-switched memory B cells with

Wuhu1 Spike+, BA.1 Spike+ and cross-reactive Spike+ specificities in both

unvaccinated and vaccinated individuals before and after BA.1 infection. Lines connect

the same individual from pre-infection frequency to post-infection frequency. P values

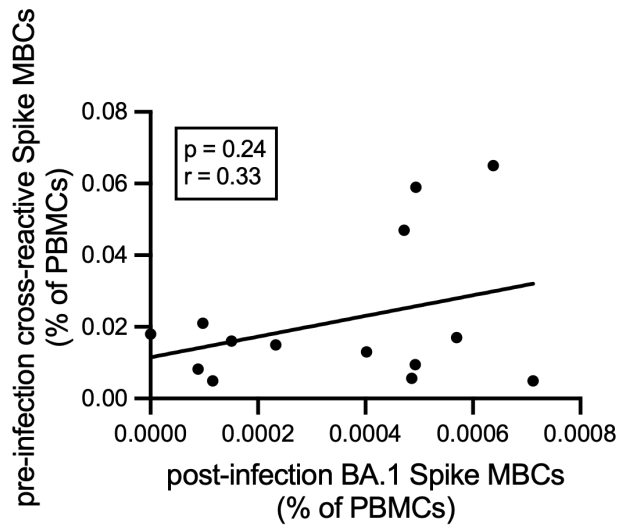
were calculated using Wilcoxon matched-pairs signed rank test on each row and post

hoc testing for multiple comparisons between draws was performed using two-stage

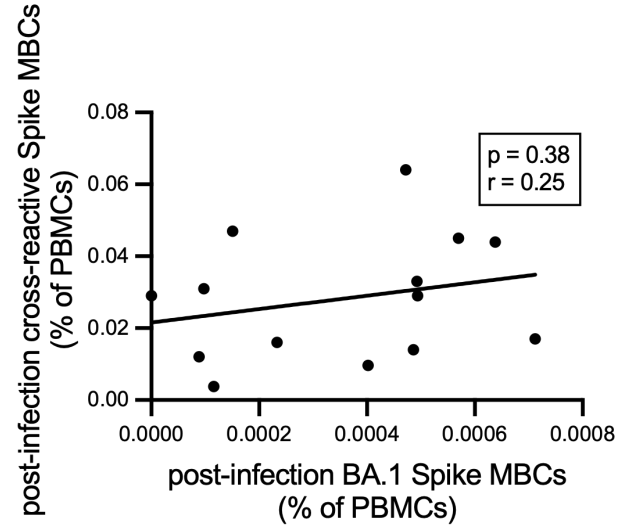
linear step-up procedure of Benjamini, Krieger and Yekutieli. P values greater than 0.05

are not depicted.

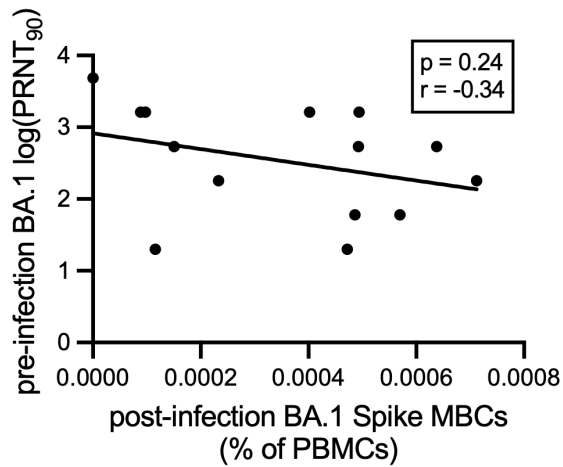
A.



B.



C.



D.

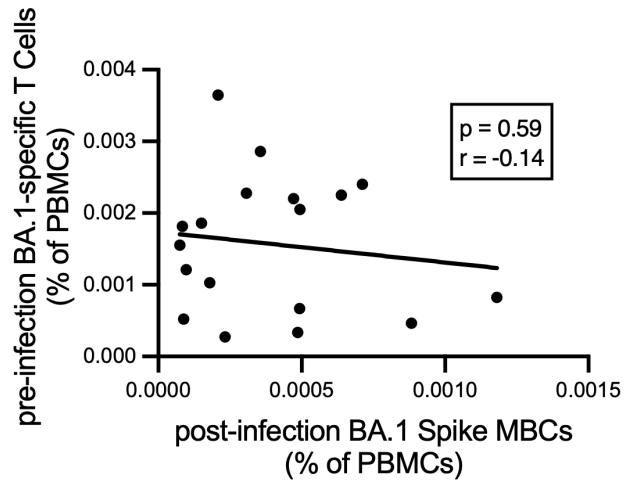
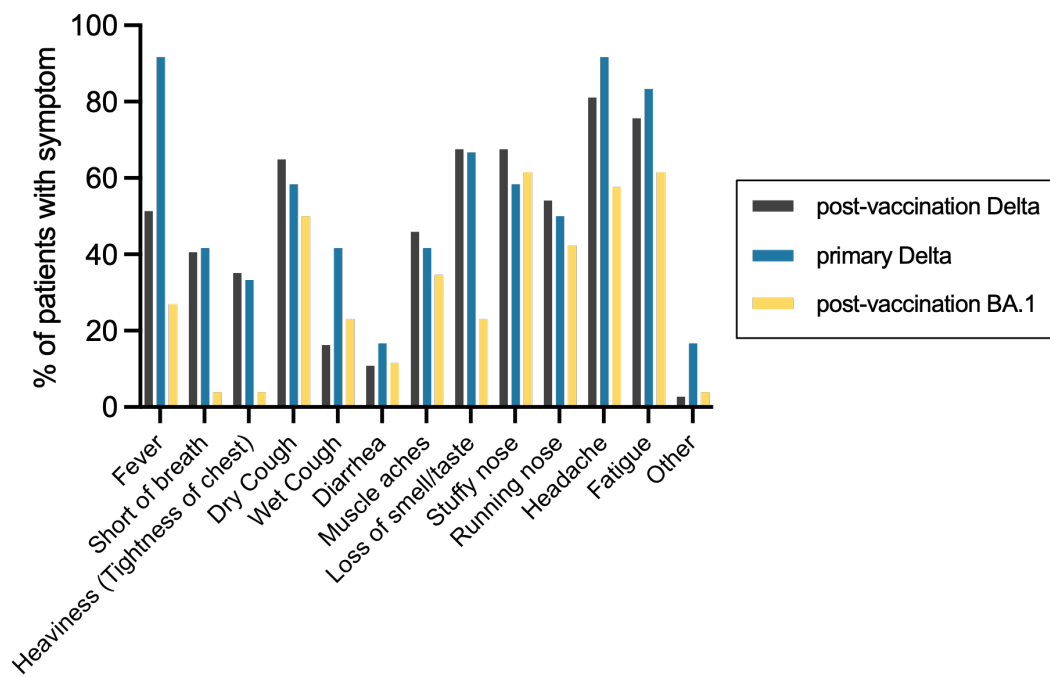


Figure 7. Correlations of pre-infection and post-infection BA.1-specific antibody, T and B cell responses. (A) Correlation of pre-infection cross-reactive Spike MBCs (calculated as in Figure 5C) plotted against the frequency of post-infection BA.1 Spike MBCs (calculated as in Figure 5C) in individuals that experienced a post-vaccination BA.1 infection. Pearson correlation analysis was performed. Pre-infection blood draws were taken on average 87.6 days before infection and post-infection draws were taken an average of 38.3 days after infection. Individuals that received a vaccine after the pre-infection draw were excluded from analysis. **(B)** Correlation of post-infection cross-reactive Spike MBCs (calculated as in Figure 6B) plotted against the frequency of post-infection BA.1 Spike MBCs (calculated as in Figure 5C) in individuals that experienced a post-vaccination BA.1 infection. Pearson correlation analysis was performed. **(C)** Correlation of pre-infection BA.1 neutralizing antibody titer (calculated as in Figure 4a) plotted against post infection BA.1 Spike MBCs (calculated as in Figure 5c) in individuals that experienced a post-vaccination BA.1 infection. Pearson correlation analysis was performed. **(D)** Correlation of pre-infection BA.1 Spike-specific T cells as measured by IFN γ ELISPOTs plotted against post-infection BA.1 Spike MBCs in individuals that experienced a post-vaccination BA.1 infection. Pearson correlation analysis was performed.

A.



B.

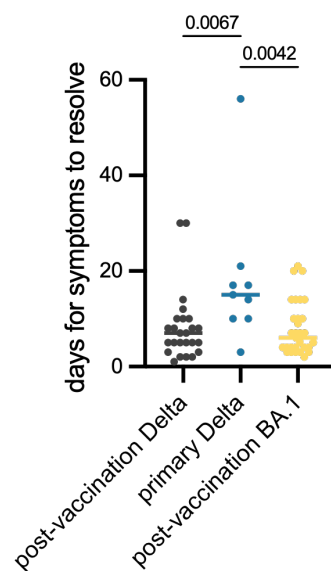
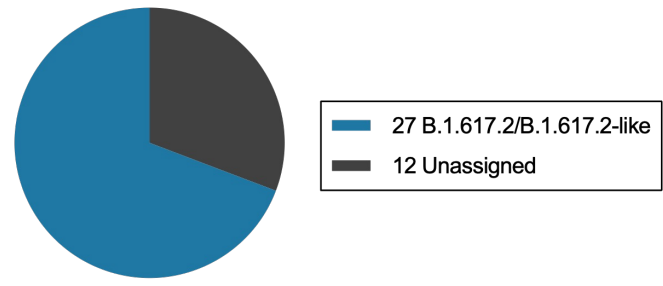


Figure S1. Test All, Test Smart (TATS) symptom report. (A) Percentage of individuals from each TATS cohort that reported experiencing various respiratory/cold symptoms in study entry survey. **(B)** Reported days until symptoms resolved for each TATS cohort. Two-sided P values from t-test statistics were calculated for pairwise differences using one-way ANOVA. Post hoc testing for multiple comparisons between draws was performed using Tukey's multiple comparisons test. P values greater than 0.05 are not depicted.

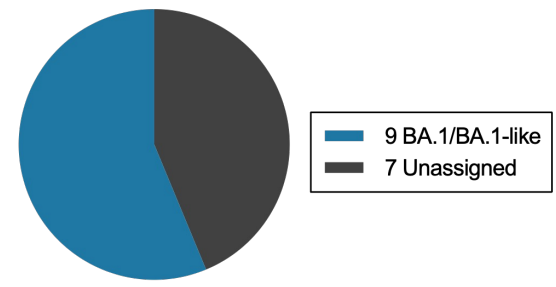
A.

TATS Delta cohort PANGO-lineages



Total=39

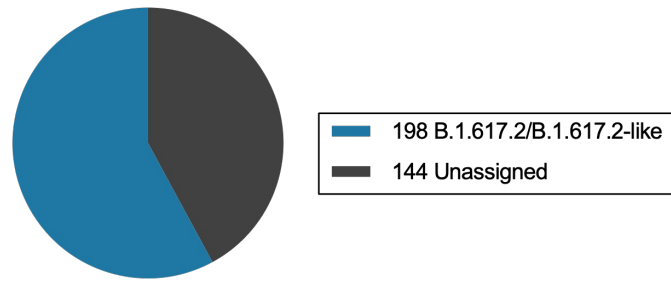
TATS BA.1 cohort PANGO-lineages



Total=16

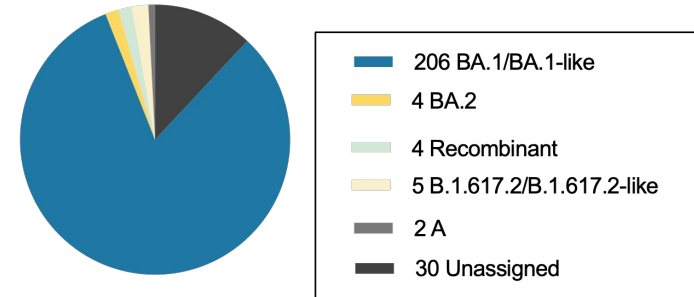
B.

TATS PANGO-lineages during Delta recruitment period (July 1, 2021-December 1, 2021)



Total=342

TATS PANGO-lineages during BA.1 recruitment period (January 1, 2022 -March 31, 2022)



Total=251

Figure S2. PANGO-lineage assignments from TATS PCR positive individuals. (A)

Delta or BA.1 PANGO-lineage assignments after SARS-CoV-2 viral amplicon sequencing (Integrated DNA Technologies). Unassigned sequences could not be assigned to a PANGO-lineage due to insufficient viral RNA recovery and low sequence coverage. **(B)** PANGO-lineage assignments of all TATS samples submitted during the period of Delta cohort recruitment, July 1, 2021-December 1, 2021 (left panel) or during the period of BA.1 cohort recruitment, January 1, 2022-March 31, 2022 (right panel). Unassigned sequences could not be assigned a lineage due to insufficient viral RNA recovery and low sequence coverage.

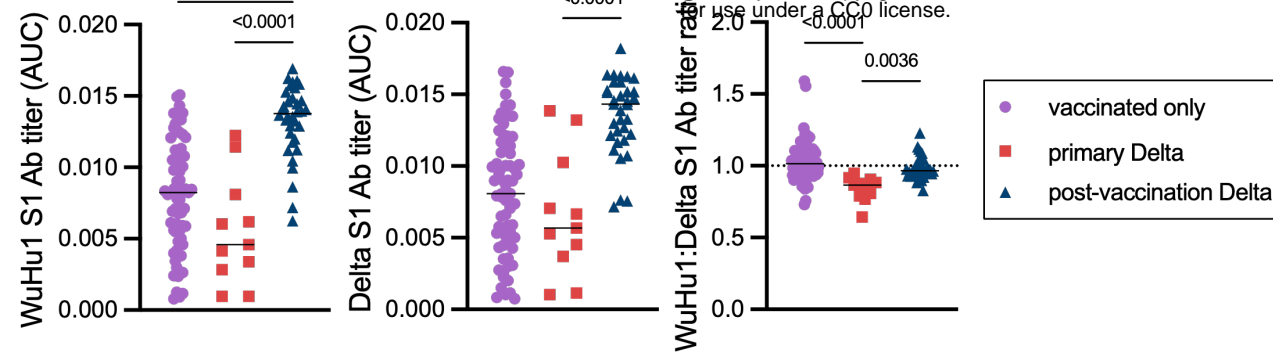
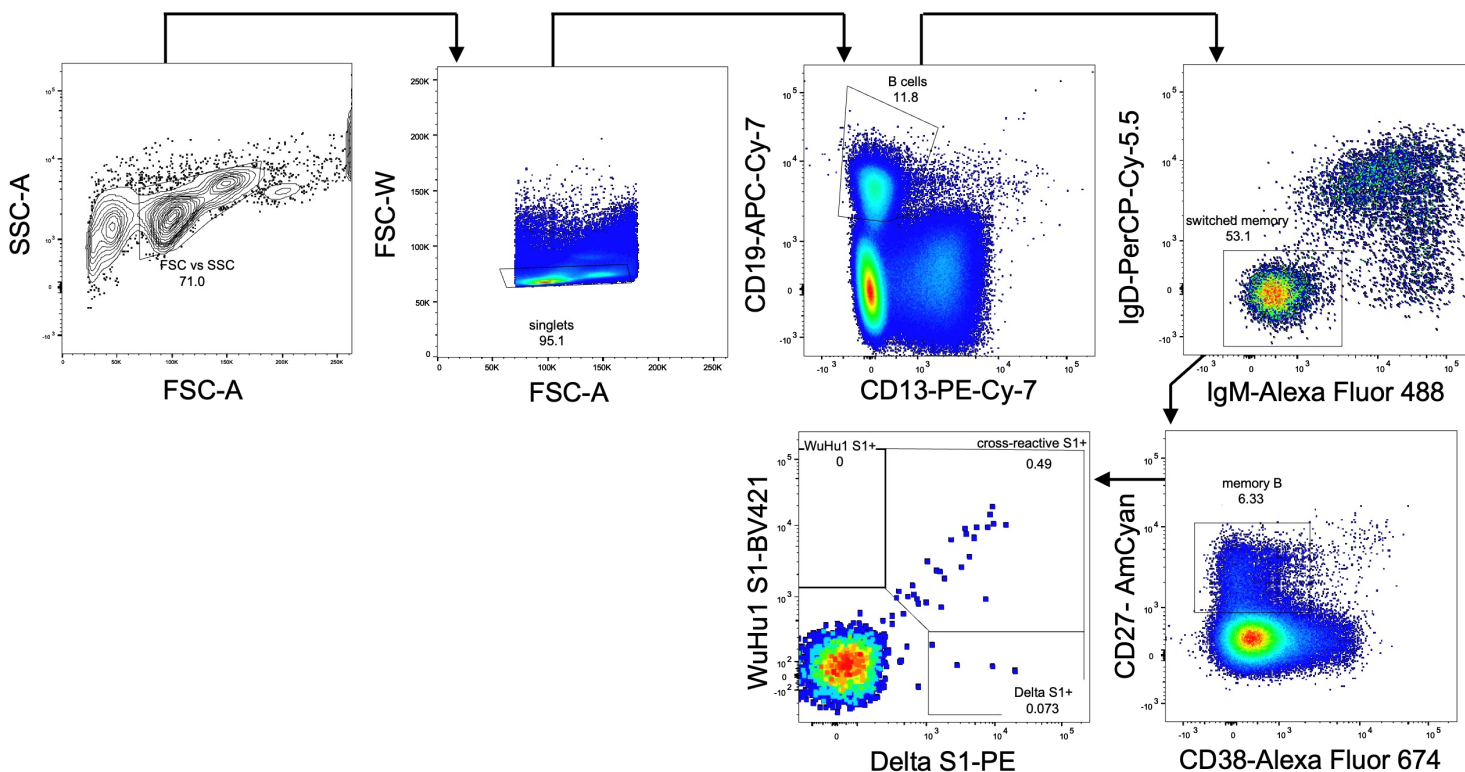
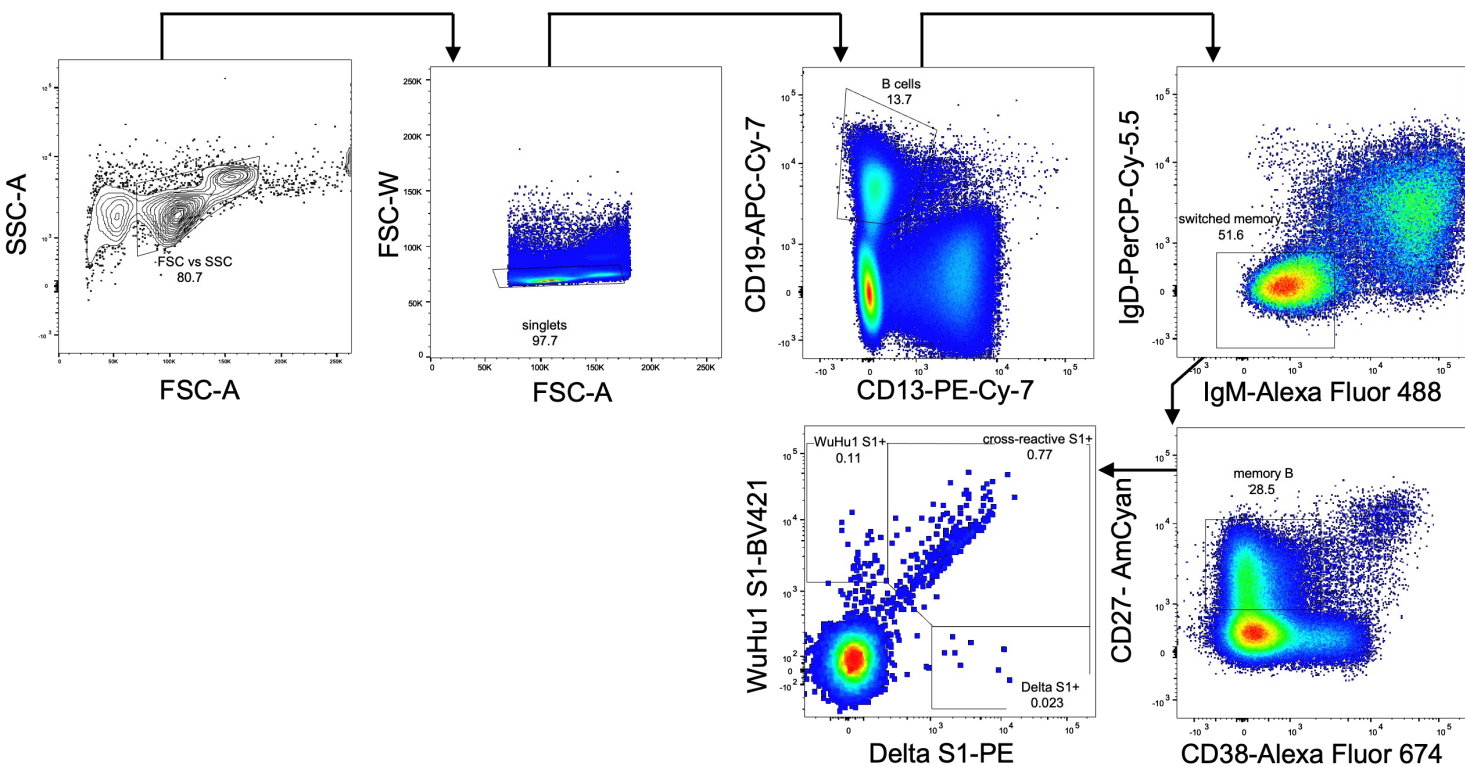


Figure S3. Primary and recall antibody responses to Wuhan and Delta strains of SARS-COV-2. Quantitative titers of WuHu1- and Delta S1-specific antibodies. Serum was initially diluted 1:60, serially diluted 1:3, assessed by ELISA for binding to the listed antigens, and area under the curve (AUC) values were calculated. Each symbol represents an individual. WuHu1 AUC values were divided by their Delta AUC titer in the same individual to calculate a WuHu1:Delta S1 ratio in the rightmost panel. Two-sided P values from t-test statistics were calculated for pairwise differences using one-way ANOVA. Post hoc testing for multiple comparisons between draws was performed using Tukey's multiple comparisons test. P values greater than 0.05 are not depicted.

primary Delta



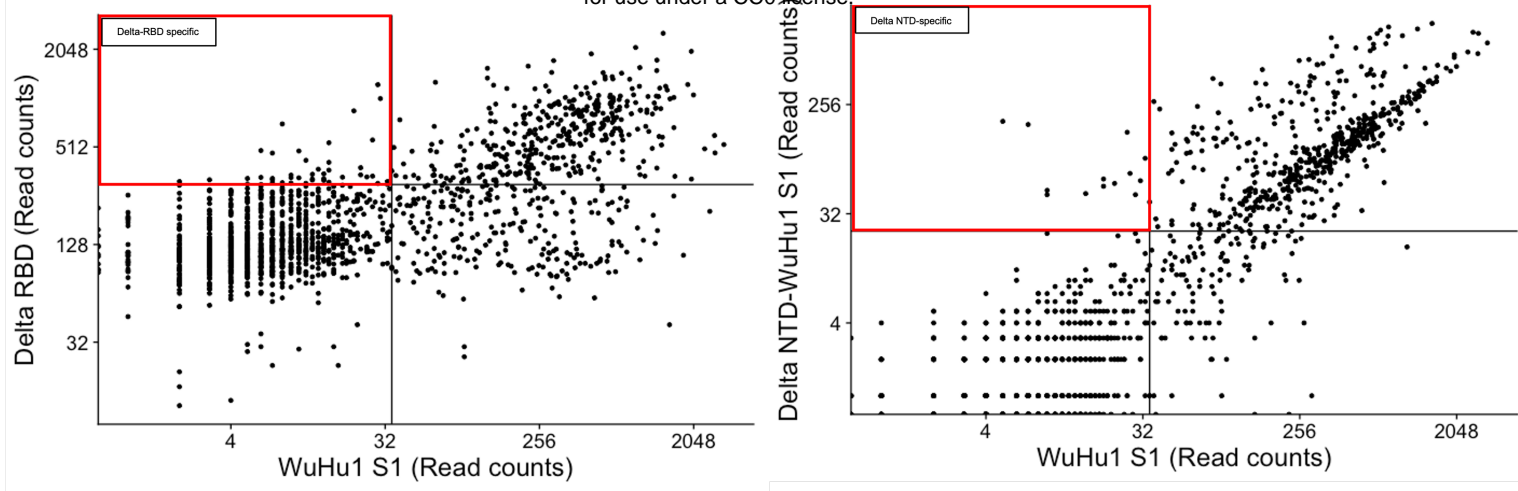
post-vaccination Delta



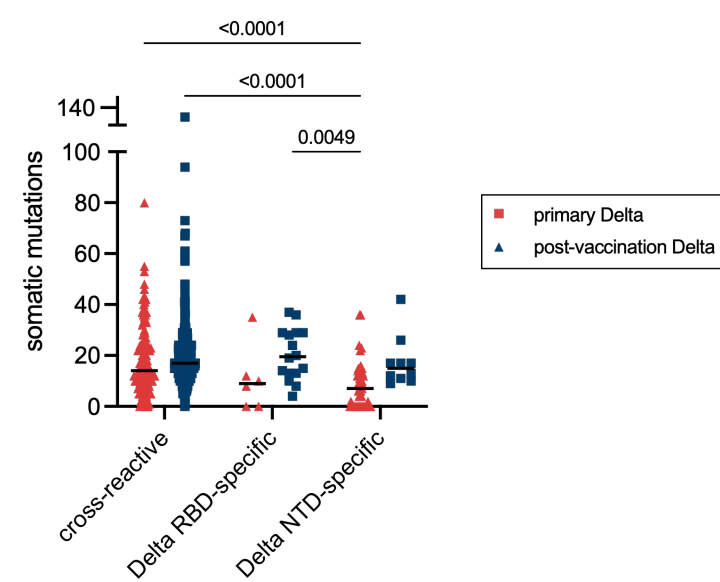
1323 **Figure S4. Flow cytometric gating strategy with Delta S1 and WuHu1 S1**
1324 **tetramers.** Examples of a sample from a primary Delta infection (top) and post-
1325 vaccination Delta infection (bottom) are shown.
1326

Figure S5

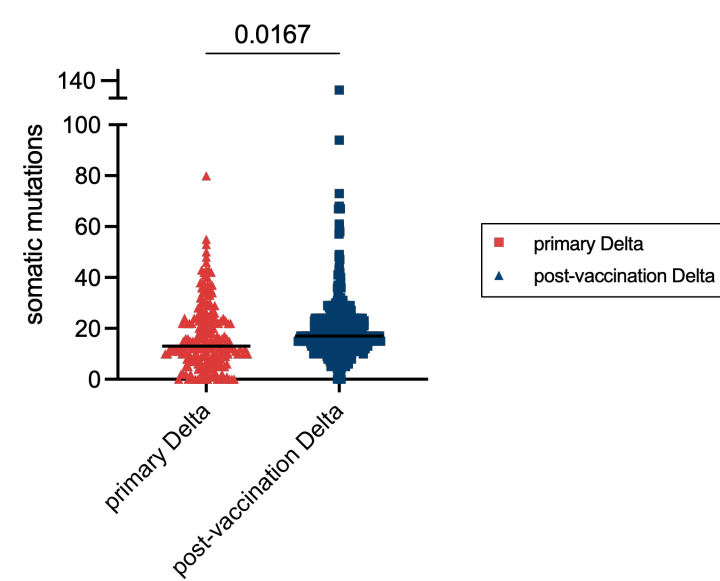
A.



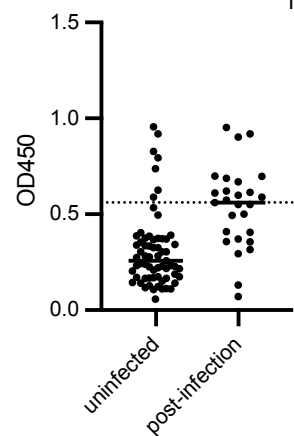
B.



C.



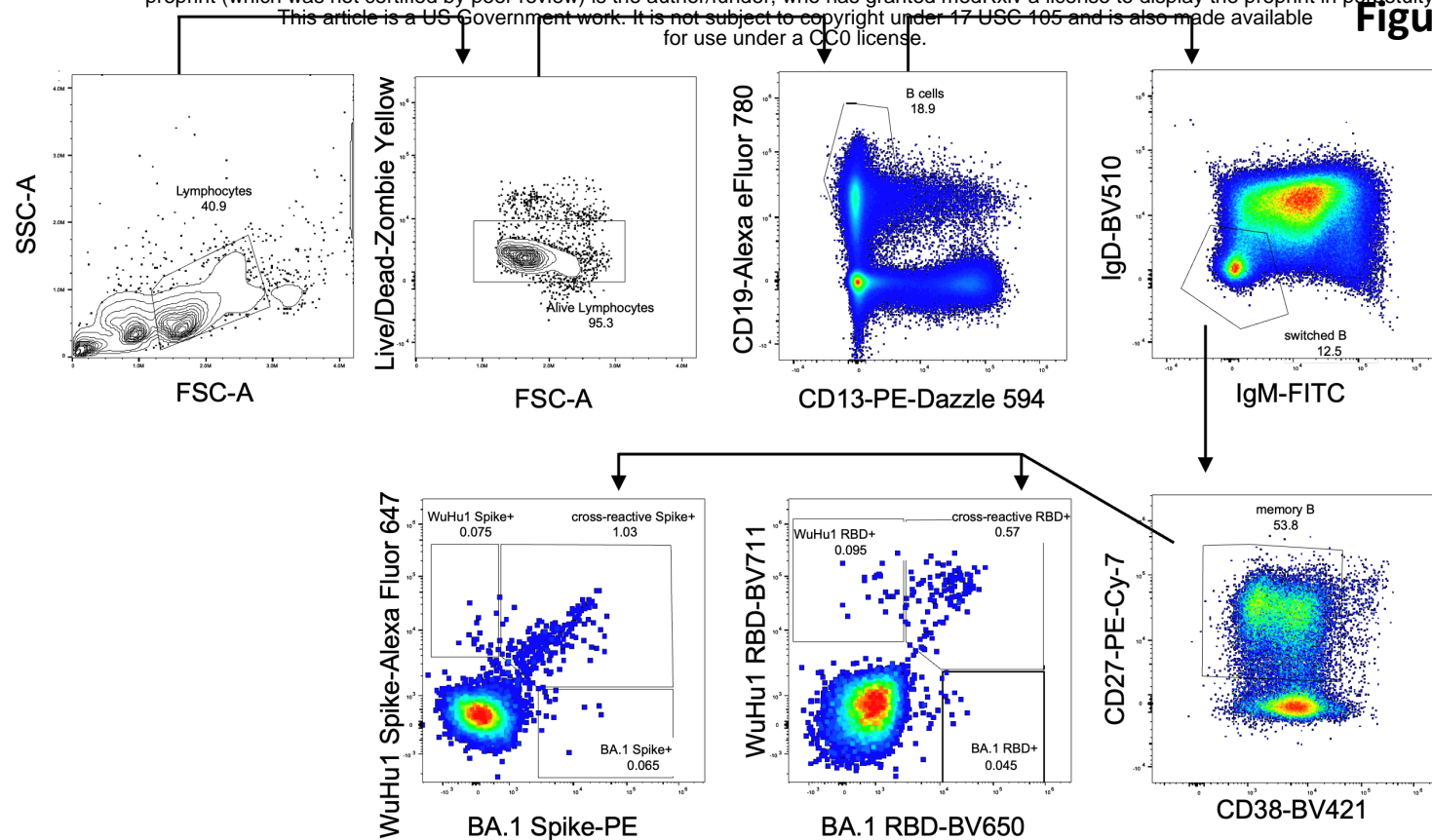
Figures S5. LIBRA-seq analysis in post-vaccination Delta infections and quantification of somatic mutations. (A) A chimeric protein (Delta NTD-WuHu1 S1) was generated in which Delta NTD mutated epitopes (T19R, G142D, E156-, F157-, R158G) were incorporated into the otherwise WuHu1 S1 backbone. Quantification of Delta RBD-specific (**left**) and Delta NTD-specific memory B cells (**right**) in individuals that experienced a post-vaccination Delta infection. Delta RBD-specific cells were classified by cells that had Delta RBD read counts of greater than 300 and WuHu1 S1 read counts of less than 35. Delta NTD-specific cells were classified by cells that had Delta NTD-WuHu1 S1 read counts of greater than 23 and WuHu1 S1 read counts of less than 35. Read count thresholds to determine positivity were set using samples in which cells lacking Spike-binding specificities were sorted and sequenced. Plots are concatenated from ten individuals. **(B)** Somatic mutations were calculated using the observedMutations command in the Shazam Immcantation package in R. Specificities of cells are determined using the same cutoffs described in **Figure S3A and 3D. (C)** Quantification of somatic mutations of all Spike specific cells subjected to scRNAseq from either ten post-vaccination or primary Delta infections.



1348 **Figure S6. anti-Nucleocapsid titers in uninfected individuals.** Individuals with α -
1349 Nucleocapsid titers of greater than 0.6 at a 1:60 serum dilution were considered
1350 previously infected and excluded from the study.

1351

1352



1353 **Figure S7. Flow cytometric gating strategy with BA.1 RBD, BA.1 Spike, WuHu1**

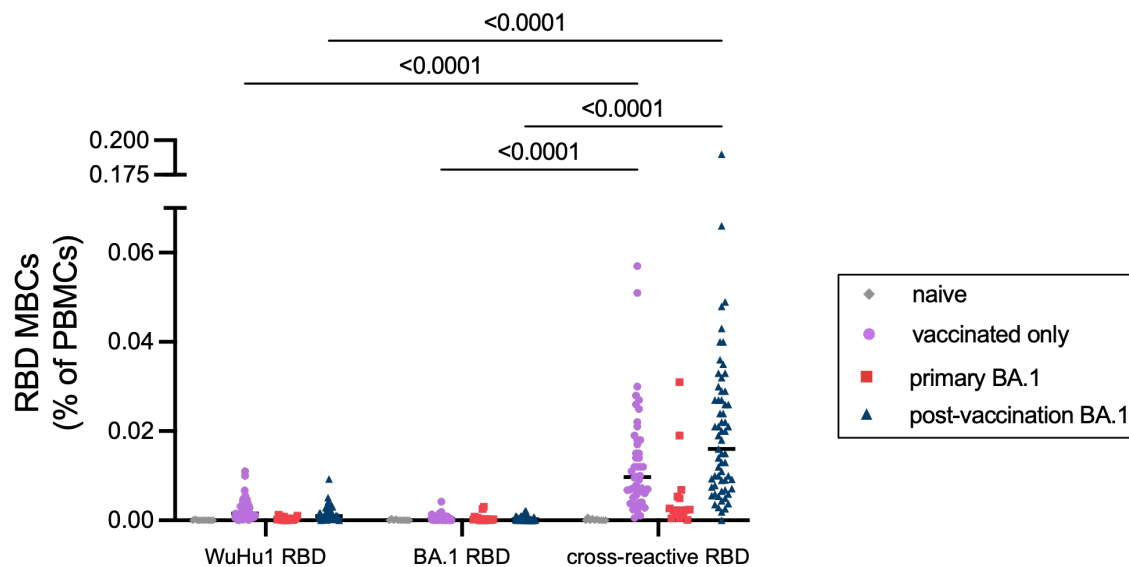
1354 **RBD and WuHu1 Spike tetramers.** An example of a sample from a post-vaccination

1355 BA.1 infection is shown.

1356

1357

A.



B.

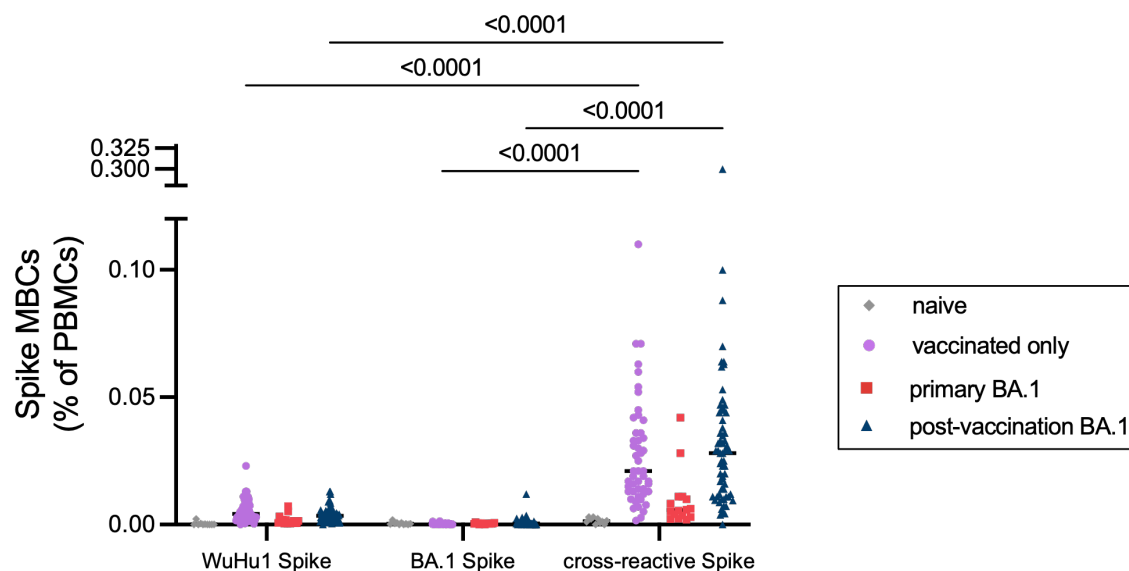


Figure S8. WuHu1 and BA.1 Memory B cell flow cytometric quantification. (A)

Cells that bind both WuHu1 RBD and BA.1 RBD are annotated as cross-reactive RBD+, whereas cells that bind only WuHu1 RBD or BA.1 RBD are annotated as WuHu1 RBD+ or BA.1 RBD+, respectively. Quantification of isotype-switched memory B cells as a percentage of total PBMCs for WuHu1 RBD+, BA.1 RBD+ and cross-reactive RBD+ specificities for each cohort of SARS-CoV-2 immune histories. Each symbol represents an individual. Two-sided P values from t-test statistics were calculated for pairwise differences using two-way ANOVA. Post hoc testing for multiple comparisons between draws was performed using Tukey's multiple comparisons test. P values greater than 0.05 are not depicted. **(B)** Cells that bind both WuHu1 RBD and BA.1 Spike are annotated as cross-reactive Spike+, whereas cells that bind only WuHu1 Spike or BA.1 Spike are annotated as WuHu1 Spike+ or BA.1 Spike+, respectively. Quantification of isotype-switched memory B cells for WuHu1 Spike+, BA.1 Spike+ and cross-reactive Spike+ specificities for each cohort of SARS-CoV-2 immune histories. Each symbol represents an individual. Two-sided P values from t-test statistics were calculated for pairwise differences using two-way ANOVA. Post hoc testing for multiple comparisons between draws was performed using Tukey's multiple comparisons test. P values greater than 0.05 are not depicted.

Table 1

	vaccinated only (statewide antibody testing initiative) (n=74)	primary Delta (n=12)	post-vaccination Delta (n=37)	vaccinated only (TATS) (n=62)	primary BA.1 (n=69)	post- vaccination BA.1 (n=62)
Age Mean (s.d.)	38.0 (32.0, 54.0)	21.9 (20.2, 40.7)	23.3 (18.6, 65.8)	31.9 (18.6, 65.0)	44 (25, 62)	40 (19, 71.5)
Sex						
Male	22 (32%)	5 (42%)	8 (22%)	24 (39%)		24 (39%)
Female	52 (68%)	7 (58%)	29 (78%)	37 (60%)		34 (55%)
Prior COVID infection						
Yes		12 (100%)	37 (100%)		69 (100%)	64 (100%)
No	74 (100%)					
Time since COVID infection		67.5 days (32, 99.3)	71.5 days (48.5, 89.5)		40 days (31, 44.5)	54.4 days (34.5, 71)
paired pre- and post- infection samples					10	21
Time from vaccination to pre- infection draw						138 (32.5, 217)
Time from pre- infection draw to infection					73.3 days (30, 99)	112 days (33, 187)
Time from infection to post- infection draw					42.7 days (29.5, 47.5)	44.8 days (34, 49.3)
COVID Vaccination						
# of shots	37	0	37	62	0	62
2	37 (100%)		37 (100%)	16 (26%)		13 (20%)
3				46 (74%)		15 (23%)
4						3 (5%)
time since vaccination	135.6 days (126, 270)		273.9 days (56, 317)	176.0 days (113.5, 188)		192.2 days (107, 302.3)

1377 **Table 1. Characteristics of cohorts**

1378 Interquartile range (IQR) is listed in parentheses unless otherwise stated in the table.

1379